Master's Thesis of Science
in Food Science and Biotechnology

The structure and activation mechanism of itaconic acid-responsive transcriptional regulator RipR in the pathogenesis of foodborne pathogen

식품병원균 유래 이타콘산 반응 전사조절인자
RipR 의 구조 및 활성화 분자 기전

August 2022

Food Science and Biotechnology Major
Department of Agricultural Biotechnology
The Graduate School
Seoul National University

Nayeon Ki

석사학위논문

The structure and activation mechanism of itaconic acid-responsive transcriptional regulator RipR in the pathogenesis of foodborne pathogen

지도교수 하 남 출

이 논문을 석사학위논문으로 제출함

2022 년 8 월

농생명공학부 식품생명공학전공
서울대학교 대학원
기 나 연

기나연의 석사학위논문을 인준함
2022 년 8 월

위원장	이 도 엽	(인)
부위원장	하 남 출	(인)
위원	이 주 훈	(인)

Abstract

Macrophages produce itaconic acid in phagosomes in response to LPS to eliminate invading pathogenic bacteria. Itaconic acid competitively inhibits the first enzyme of the bacterial glyoxylate cycle. To overcome itaconic acid stress, bacteria employ the bacterial LysR-type transcriptional regulator RipR. However, it remains unknown which molecule activates RipR in bacterial pathogenesis. In this study, we determined the crystal structure of the regulatory domain (RD) of RipR from the intracellular pathogen *Salmonella*. The RipR RD structure exhibited the typical dimeric arrangement with the putative ligand binding site between the two subdomains. The ITC experiments identified isocitrate as the physiological ligand of RipR, whose intracellular level is increased in response to itaconic acid stress. We further found that 3-phenylpropionic acid significantly decreased the resistance of the bacteria to itaconic acid challenge. Consistently, the complex structure revealed that the compound is antagonistically bound to the RipR ligand binding site. This study provides the molecular basis of bacterial survival in itaconic acid stress from our immune systems. Further studies are required to

reveal biochemical activity, which would elucidate how *Salmonella* survives in macrophage phagosomes by defending against itaconic acid inhibiting bacterial metabolism.

Keywords: itaconic acid, LysR-type transcriptional regulator, isocitrate, glyoxylate cycle, 3-phenylpropionic acid, crystal structure

Student Number: **2020-25807**

Contents

List of Figures

List of Table

I. Introduction

Macrophages are activated upon inflammatory signals, such as the bacterial cell wall component LPS, and kill the invading bacteria in their phagosome with diverse antimicrobial substances, such as H_2O_2 and HOCl (Hassett and Cohen, 1989; David and Kroner, 2011). Itaconic acid (2-methylenesuccinic acid), an unsaturated dicarboxylic acid, was recently noted as a new antibacterial substance in the macrophage phagosome (Cordes *et al.*, 2015). Itaconic acid is generated from the precursor cis-aconitate by the enzymatic activity of the immune-responsive gene 1 (Irg1) gene product, which is the most highly upregulated by the bacterial cell wall component LPS in macrophages (Basler *et al.*, 2006; Thomas *et al.*, 2006; Degrandi *et al.*, 2009; Tangsudjai *et al.*, 2010; Gautam *et al.*, 2011; Cordes *et al.*, 2015; Coelho, 2022). The antimicrobial activity of itaconic acid results from the inhibition of bacterial isocitrate lyase, which catalyzes the conversion of isocitrate to glyoxylate and succinate as the key enzyme in the glyoxylate shunt pathway or the glyoxylate cycle (McFadden and Purohit, 1977). The glyoxylate cycle is widely found in bacteria, protists, fungi, and plants as a variation of the TCA cycle (Chew *et al.*, 2019; Chew and Than, 2021). The glyoxylate cycle saves two carbons by bypassing the two decarboxylation reactions (isocitrate to α-

ketoglutarate and α-ketoglutarate to succinyl-CoA) in the TCA cycle, and thus is usually employed under limiting carbon source conditions (Cronan and Laporte, 2005).

Gram-negative bacteria have LysR-type transcriptional regulators (LTTRs) to properly regulate gene expression by recognizing signaling molecules in response to diverse environmental and physiological stimuli (Lahiri *et al.*, 2009). LTTRs consist of the N-terminal DNA-binding domain (DBD) and the C-terminal regulatory domain (RD) exhibiting typical asymmetric tetrameric assembly (Maddocks and Oyston, 2008). Binding of the cognate ligands to the RD triggers the changes in transcriptional activity via structural changes in the tetrameric assembly (Jo *et al.*, 2015; Jo *et al.*, 2019). The LTTR RipR was identified as the vital component of the resistance to the antimicrobial function of itaconic acid in many gram-negative pathogenic bacteria (Hersch and Navarre, 2020). RipR activated the expression of the three enzymes r*ipC, ripB*, and *ripA*, which degrade itaconic acid in many other pathogens including *Yersinia pestis*, *Pseudomonas aeruginosa*, *Mycobacterium tuberculosis* and *Salmonella enterica*. (Menage and Attree, 2014; Sasikaran *et al.*, 2014; Cordes *et al.*, 2015). In *S. enterica*, the drastic upregulation of *ripCBA* by itaconic acid was observed through a

GFP reporter assay (Hersch and Navarre, 2020). RipR contributed to the bacterial resistance to itaconic acids in *S. enterica* and *Y. pestis* (Sasikaran *et al.*, 2014; Hersch and Navarre, 2020). RipR has DBD and RD similar to those of other LTTRs and is expected to form a tetrameric assembly similar to that of like typical LTTRs.

This study focuses on the food poisoning bacterium *S. enterica*, which can survive in macrophage phagosomes through diverse mechanisms (Uzzau *et al.*, 2000; Ren *et al.*, 2015; Bintsis, 2017). *S. enterica* has the transcriptional activator RipR to cope with the itaconic acid stress present in macrophage phagosomes. However, it remains unknown which molecule activates RipR in the defense against the itaconic acid challenge in the macrophage phagosomes. Herein, we determine the crystal structure of the RipR RD and discover the cognate ligand molecules of RipR. We further found that plant-derived secondary metabolites inhibit the RipR function. Furthermore, our findings indicate the role of itaconic acid as a mammalian antimicrobial metabolite.

Submitted

Journal of Biological Chemistry

II. Experimental Procedures

2.1. Plasmid construction

To overexpress the Regulatory domain (residues 87–292) of RipR wild type, the gene encoding the protein was amplified by polymerase chain reaction (PCR) using the following two primers. The underlined sequences represent the NcoI and XhoI restriction sites, respectively.

(Forward: 5'- GGCCCATGGCGAGGGGGGAGTCGGGCGTG-3')

(Reverse: 5'- GGCCTCGAGTCAGCCAGTGACTTTCAGGATG-3')

The amplified product and the expression vector pProEX-HTa (Invitrogen, USA) were digested with NcoI and XhoI restriction enzymes. The digested PCR product was inserted into the digested expression vector pProEX-HTa by DNA ligase. The resulting plasmid encodes the hexahistidine tag and the TEV protease cleavage site at the N-terminus of the protein. The plasmids encoding RipR wild type protein were transformed into the *Escherichia coli* C43 (DE3) strain by the heat-shock method. The recombinant plasmid was confirmed by DNA sequencing.

2.2. Purification of RipR RD and 3-phenylpropionic acid-bound RipR RD

2.2.1. Overexpression

The PCR-amplified RipR RD gene from *Salmonella enterica* was inserted into the pProEx-HTa vector (Thermo Fisher Scientific) with a hexahistidine tag and the tobacco etch virus (TEV) protease cleavage site at the N-terminus of the RipR RD. The plasmids were transformed into the *E. coli* BL21 (DE3) strain, and subsequently cultured in LB medium containing 100 μg/ml ampicillin at 37 °C. The RipR RD protein was induced at an optical density at 600 nm (OD_{600}) of 1.0 by 0.5 mM isopropyl β-D-1-thiogalactopyranoside (IPTG) with a subsequent 6-h incubation at 30 °C. The harvested cells were resuspended in 50 ml of lysis buffer composed of 20 mM HEPES (pH 7.0), 300 mM sodium chloride, and 2 mM β-mercaptoethanol. The cells were disrupted using a French press (Constant Systems Limited, United Kingdom) at a pressure of 23 kpsi, and were cleared by centrifugation at 19,000 × *g* for 30 min at 4 °C. The crude lysate was centrifugated at 19,000 g for 30 min at 4°C and the pellet containing cell debris was discarded.

2.2.2. Affinity chromatography

The supernatant was loaded onto nickel-nitrilotriacetic acid affinity agarose resin (GE Healthcare) in lysis buffer and rolled in a column for 50 min at 4°C. The RipR RD protein was eluted with 250 mM imidazole in lysis buffer. After washing the column with ~300 mL lysis buffer supplemented with 20 mM imidazole, the RipR RD protein was eluted with lysis buffer supplemented with 250 mM imidazole. The eluate was treated with recombinant TEV protease by incubation at room temperature for 12 h to cleave the hexahistidine tag. The cleaved proteins purified by flowing through an anion exchange chromatographic column (HiTrap Q column; GE Healthcare).

2.2.3. Size exclusion chromatography (SEC) and concentration

The flow-through proteins were concentrated using a Vivaspin centrifugal concentrator (30 kDa molecular-weight cutoff; Millipore, USA) and loaded on a Superdex 200 HiLoad 26/600 column (GE Healthcare) in lysis buffer for size exclusion chromatography equilibrated with 20 mM HEPES (pH 7.0) buffer containing 300 mM NaCl and 2-mercaptoethanol. The purified protein

was concentrated up to 13 mg/mL using Vivaspin 20 (Sartorius, Germany) and stored at –80°C. The final protein concentration was 15 mg/ml.

2.3. Crystallization of RipR RD and 3-phenylpropionic acid-bound RipR RD

RipR proteins (RipR RD, 3-phenylpropionic acid-bound RipR RD) were crystallized at 16°C using the hanging drop vapor diffusion method after mixing 1 µl protein solution and 1 µl precipitation solution. The initial crystallization trials of the purified 3-phenylpropionic acid-bound RipR RD and ligand-free RipR RD protein were performed in a MOSQUITO automated crystal screening device at 14 °C with a sitting-drop vapor-diffusion method. The RipR RD crystals were obtained with the hanging-drop diffusion method under a reservoir solution containing 0.2 M sodium formate (pH 5.75) and 19% (w/v) polyethylene glycol 3,350 at 14 °C in a 15-well plate. The crystals of RipR RD in complex with 3-phenylpropionic acid were obtained under a reservoir solution containing 0.1 M sodium cacodylate trihydrate (pH 6.5) and 1.4 M ammonium sulfate at 14 °C in a 15-well plate. For data collection, the crystals of ligand-free RipR RD and 3-

phenylpropionic acid -bound RipR RD were transferred to 2 µl of Cryo Mix 4 (CryoProtX^{tm}), and 20% (vol/vol) glycerol, respectively, and incubated for 10 sec. Then crystals were flash-cooled in liquid nitrogen at -173 °C for data collection.

2.4. Data collection and structural determination

The datasets were collected at wavelength of 1.04477 Å and 0.97957 Å on an ADSC quantum Q270 CCD detector in beamline 11C of the Pohang Accelerator Laboratory, Republic of Korea. The program HKL2000 was used to process, merge, and scale the diffraction datasets (Otwinowski and Minor, 1997). Table 1 describes the data-collection statistics. X-ray diffraction data were processed using HKL2000 software (Otwinowski and Minor, 1997). The structure of ligand-free RipR RD was determined by the molecular replacement method using the program MOLREP (Vagin and Teplyakov, 2010) in the CCP4 package (Winn *et al.*, 2011). The model structure was generated by the programs AlphaFold2 (Jumper *et al.*, 2021; Varadi *et al.*, 2022) and ColabFold (Mirdita *et al.*, 2022). The ligand-free RipR RD was refined using the software programs PHENIX refine (Adams *et al.*, 2010) and Coot (Emsley

et al., 2010). The structures of 3-phenylpropionic acid-bound RipR RD were determined using the ligand-free structure. The final structures of RipR RD were refined using the PHENIX software suite (Adams *et al.*, 2010).

2.5. Size exclusion chromatography – multiangle light scattering

The sizes of the RipR RD protein were assayed using SEC-MALS. A high-performance liquid chromatography pump (Agilent, USA) was connected to a Superdex-200 10/300 GL gel filtration column (GE Healthcare) and a MALS instrument (Wyatt Dawn Heleos, USA). The size-exclusion chromatography column was preequilibrated with buffer containing 20 mM HEPES (pH 7.0), 300 mM NaCl, and 2 mM β-mercaptoethanol for RipR RD. Bovine serum albumin (2 mg/ml) was used as the standard. RipR RD (2 mg/ml) was injected onto the column and eluted at a flow rate of 0.2 ml/min. The datasets were evaluated using the Debye model for fitting static light-scattering data, and refractive index peaks were presented in EASI graphs created using Astra V software (Wyatt Dawn Heleos).

2.6. Isothermal titration calorimetry (ITC)

MicroCal Auto ITC200 (Malvern Panalytical) at the Korea Basic Science Institute was used for the ITC experiments. All samples were prepared in a buffer containing 20 mM HEPES (pH 7.0), 300 mM sodium chloride, and 2 mM β-mercaptoethanol. The ligands, potassium threo-isocitrate, itaconic acid, sodium succinate, malic acid, sodium oxaloacetate, cis-aconitic acid, and 3-phenylpropionic acid were purchased from Sigma–Aldrich. RipR RD (30 μM) was prepared in the sample cell, and each ligand (300 μM) was loaded into a titrating syringe. The titrations were measured with 19 2-μl injections with 150-s spacing at 25 °C.

2.7. Molecular docking and molecular dynamics simulations

The molecular docking of the compounds used in the ITC analysis on the RipR RD ligand binding pocket was conducted by AutoDock Vina in PyRx virtual screening software (Dallakyan and Olson, 2015). To further refine the docked structures, we employed energy minimization and equilibrium procedures in the MD simulation program. The Gromacs software package (Hess *et al.*, 2008; Pronk *et al.*, 2013) was used for the MD simulation to evaluate RipR RD

toward the binding structure of isocitrate and docking studies of the isocitrate molecules with the protein. The topology file for protein and Gromacs files were prepared using the CHARMM36m force field in CHARMM-GUI (Jo *et al.*, 2008; Huang *et al.*, 2017). The structure was solvated in TIP3P water and neutralized by adding 150 mM KCl molecules. Protein and ligand molecules were merged for each system, solvated with TIP3P water molecules, energy minimized, and equilibrated. The system was subjected to energy minimization using the steepest descent algorithm. The minimized state was equilibrated with a 125 ps NVT simulation to attain the temperature of 310 K and a 125 ps NPT simulation for the target pressure of 1 bar. The resulting complex structure was regarded as the refined structure at 0 ns. The time step was set to 0.002 ps following a published protocol. The MD simulation was carried out for 200 ns, which was started at the endpoint of equilibration. The RMSD of the simulated structure was calculated from the trajectory data using the Gromacs tool.

2.8. Salmonella strain and growth inhibition assay

Salmonella enterica Typhimurium SL1344 was used in this study and grown at 37 °C on Luria-Bertani (LB) medium (Difco, MI, USA). The *S.* Typhimurium strain was cultured in LB medium overnight. Then, the cells were inoculated (1:100 ratio) into fresh LB media with various concentrations (0, 5, and 10 mM) of itaconic acid in a 24-well plate. After treatment with given concentrations (0, 0.1, 0.5, and 1 mM) of 3-phenylpropionic acid, the plate was incubated at 37 °C. The OD_{600} were measured with SpectaMax i3 Platform (Molecular Devices, CA, USA).

2.9. RNA extraction and quantitative real-time (qRT)-PCR

The *S.* Typhimurium strain was cultured in LB medium containing 0 or 5 mM itaconic acid at given concentrations (0, 10, 50, 100, 500, and 1000 μM) of 3-phenylpropionic acid. After incubation of the bacterial cells for 4 h at 37 °C, total RNA was extracted using an RNeasy Mini Kit (Qiagen, Germany) and its cDNA was synthesized using EcoDryTM Premix and random hexamers (Takara, Japan). The cDNA was mixed with 2 × iQ SYBR Green Supermix (Bio–Rad, CA, USA), and 0.3 μM of each primer in a 20 μl reaction volume.

The qRT-PCRs were performed in the CFX Connect™ Real-Time PCR detection system (Bio–Rad, USA) using the primer sets listed in Table 3. The transcription level of gyrB was used for normalization.

III. Results

3.1. Overexpression and Purification of RipR

RipR is commonly found in *Salmonella* and *Yersinia*. Since itaconic acid is produced in macrophage phagosomes as a major bactericidal agent, the function of RipR in resistance to itaconic acid stress suggests that RipR plays a role in the survival of the bacteria.

Sequence comparison suggested that RipR belongs to the group LysR-type transcriptional regulator (LTTR) due to the sequence similarity of common LTTR family. LTTR family proteins are involved in the regulation of various processes, including stress responses, motility, virulence, and amino acid metabolism. Members of this family have a conserved structure with an N-terminal DNA-binding domain (DBD) motif and a C-terminal ligand-binding regulatory domain (RD) motif. We studied the RipR RD to find the ligand of RipR protein.

To gain mechanistic insights on RipR RD from its 3D structures, We expressed the RD (residues 87-292) of RipR from *S. enterica* serovar

Typhimurium (*S*. Typhimurium) in the *Escherichia coli* expression system. The purified protein was crystallized in the space group of $P2_1$, and its crystal structure was determined at 2.3 Å resolution by the molecular replacement method. The search model for the molecular replacement was generated by the structural prediction program Alphafold 2 (Jumper *et al.*, 2021; Varadi *et al.*, 2022). The asymmetric unit contained four closely interacting protomers, indicating two homodimeric assemblies of the RipR RD, similar to typical LTTR RDs (Choi *et al.*, 2001; Taylor *et al.*, 2012; Jo *et al.*, 2015; Jo *et al.*, 2017; Mahounga *et al.*, 2018; Jo *et al.*, 2019) (Fig. 3 and 4). The SEC-MALS confirmed the homodimer in the solution state, as observed in many LTTR RDs (Fig. 1B).

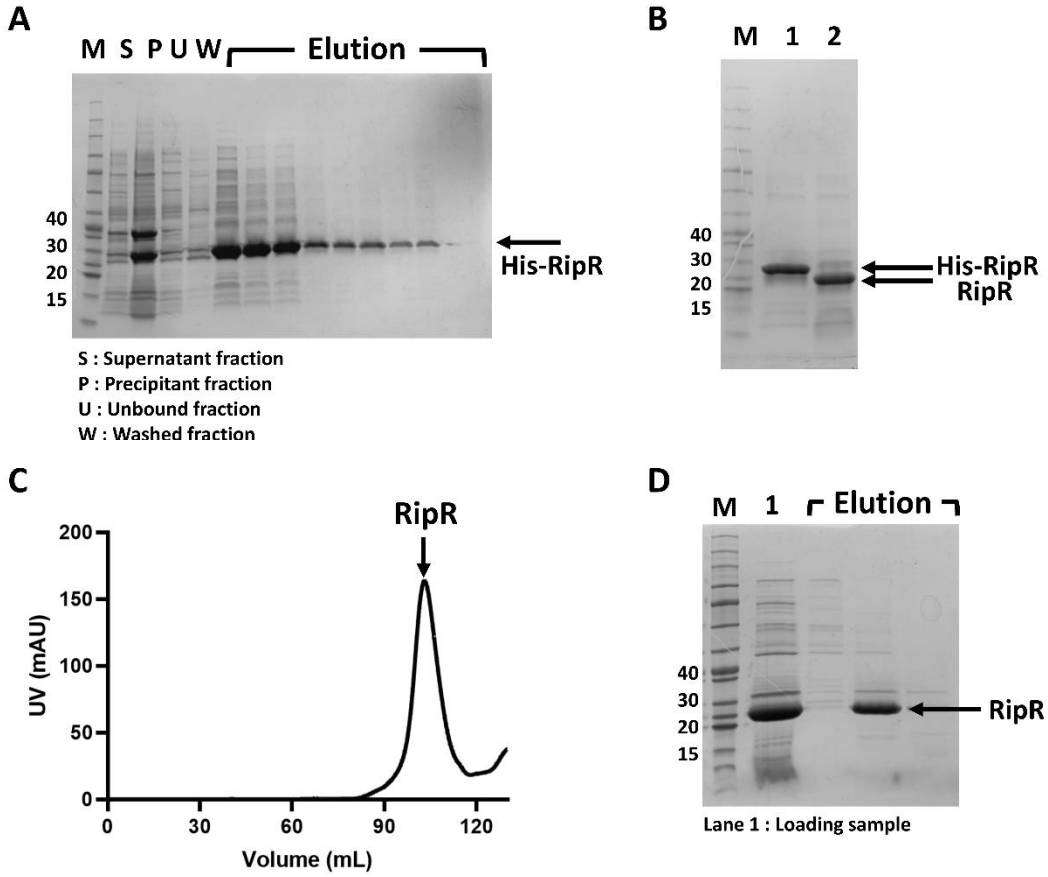

Figure 1. Purification profile of RipR RD.

A. SDS-PAGE analysis of Ni-NTA affinity chromatography

B. SDS-PAGE analysis of His-tag cleavage using TEV protease.

C. UV diagram of the superdex column elution during the size exclusion chromatography.

D. SDS-PAGE analysis of size exclusion chromatography.

3.2. Crystallization, structural determination and overall structure of RipR RD

The purified RipR RD was concentrated up to 15 mg/mL for the crystallization. The RipR RD crystals were obtained with the hanging-drop diffusion method under a reservoir solution containing 0.2 M sodium formate (pH 5.75) and 19% (w/v) polyethylene glycol 3,350 at 14 °C in a 15-well plate. The crystals of RipR RD in complex with 3-phenylpropionic acid were obtained under a reservoir solution containing 0.1 M sodium cacodylate trihydrate (pH 6.5) and 1.4 M ammonium sulfate at 14 ℃ in a 15-well plate improved the quality of RipR crystals (Fig. 2).

The crystal structure of RipR from *Salmonella enterica* was successfully determined at 2.3 Å resolution (Fig. 2 and Table 1). The crystal of RipR belongs to the space group $P2_1$, with unit cell dimensions of a=66.1 Å, b=72.4 Å, and c=91.2 Å. The The asymmetric unit contained four protomers consisting of two homodimers (Fig. 3 and 4). The SEC-MALS confirmed the homodimer in the solution state, as observed in many LTTR RDs (Fig. 5).

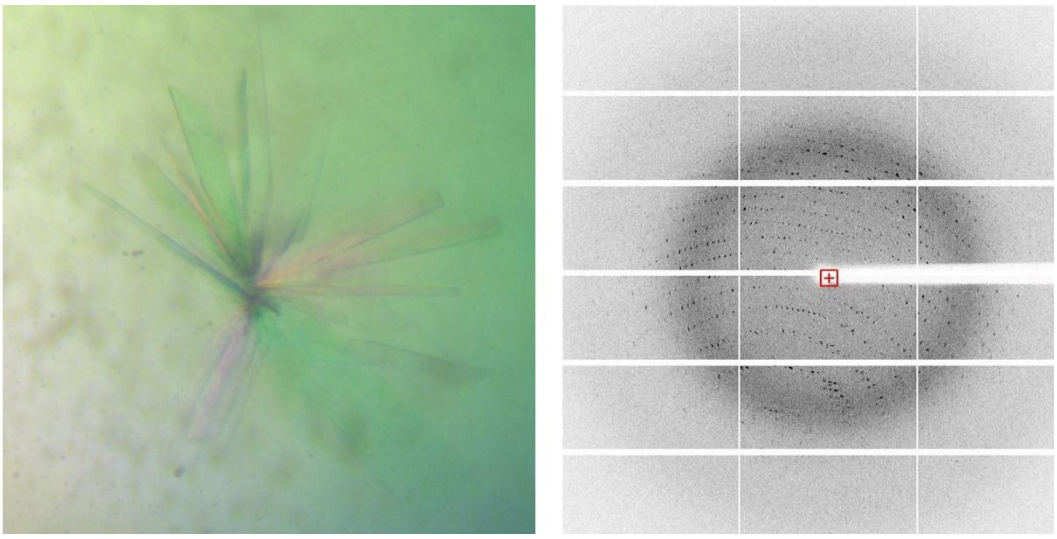

Figure 2. Crystals (left) and X-ray diffraction image (right) of RipR RD.

Table 1. Data collection and refinement statistics

	Ligand-free RipR	3-phenylpropionic acid RipR
Data collection		
Beamline	PAL 11C	PAL 11C
Wavelength (Å)	1.00919	0.97957
Space group	$P2_1$	$P3_12$
Cell dimensions		
a, *b*, *c* (Å)	66.1, 72.4, 91.2	83.1, 83.1, 172.2
α, β, γ (°)	90.0, 104.6, 90.0	90.0, 90.0, 120.0
Resolution (Å)	50.00-2.20 (2.24-2.20)	50.00-2.80 (2.90-2.80)
Total No. reflections	42,095	17,472
R_{pim}	0.043 (0.159)	0.022 (0.448)
$CC_{1/2}$	0.990 (0.905)	1.000 (0.778)
I/σ(I)	17.6 (4.4)	31.6 (2.0)
Completeness (%)	98.7 (98.2)	99.25 (99.14)

Redundancy	6.1 (5.9)	20.1 (19.3)
Refinement statistics		
Resolution (Å)	39.26-2.37	28.70-2.80
No. of reflections	32,760	17,442
R_{work}/R_{free}	0.236/0.295	0.213/0.256
No. of total atoms	6,309	3,187
No. of protein atoms	6,279	3,148
No. of water atoms	30	26
No. of other atoms	0	13
Wilson B-factor	40.09	86.29
RMSD		
Bond lengths (Å)	0.002	0.003
Bond angles (°)	0.573	0.658
Ramachandran plot		
favored (%)	97.3	94.58

allowed (%)	2.46	5.17
outliers (%)	0.25	0.25
PDB ID	7V5V	7XRO

* The values in parentheses are for the highest resolution shell.

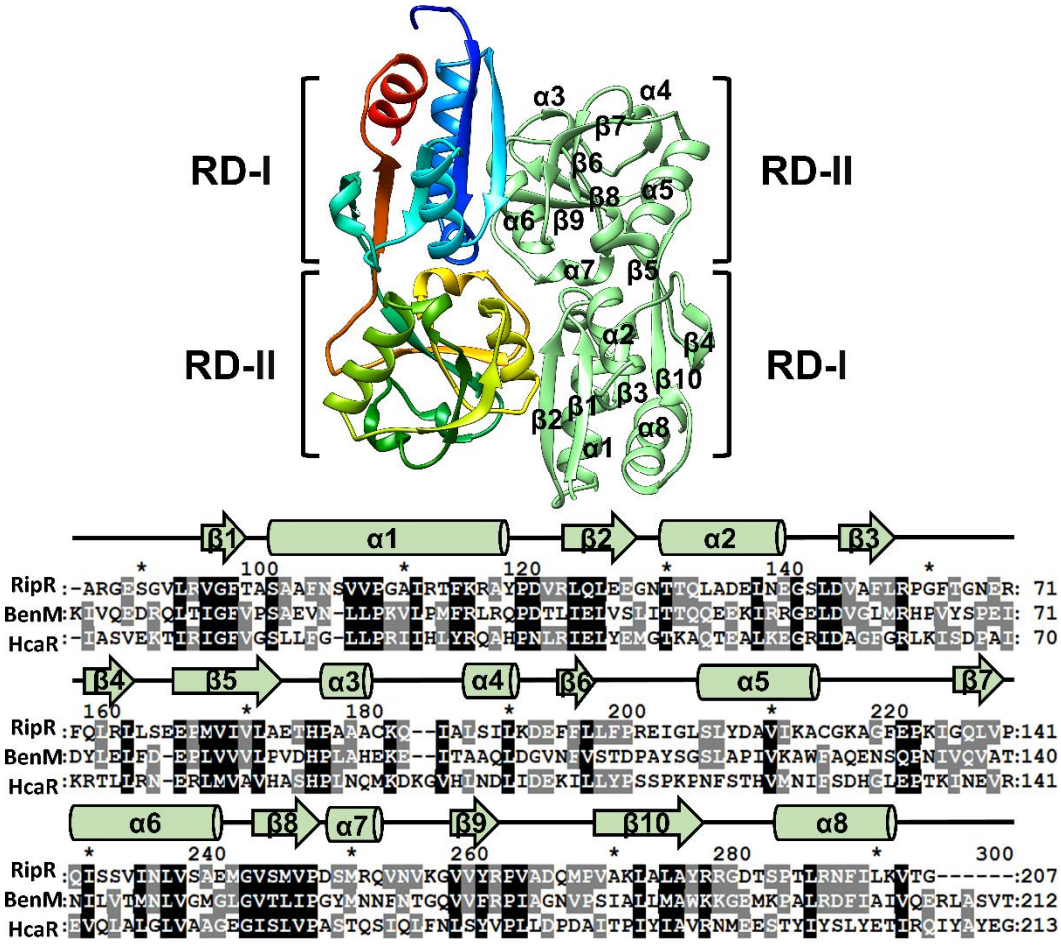

Figure 3. The structure of the dimeric assembly of RipR RD.

The asymmetric unit of the RipR RD from *S.* Typhimurium in the ribbon representations. The asymmetric unit contains two copies of the RipR RD. The protomer of RipR RD on the left side is depicted in rainbow color, while the other protomer on the right side depicted in palegreen. The subdomains RD-I and RD-II are labeled. RD-I comprises three α-helices (α1, α2, and α8), and

five β-strands (β1, β2, β3, β4, and β10). RD-II comprises five α-helices (α3, α4, α5, α6 and α7), and five β-strands (β5, β6, β7, β8, and β9). Sequence comparison of RipR to its homologs: BenM, *Acinetobacter balylyi* and HcaR, *Escherichia coli*. The secondary structural elements are annotated above the sequence.

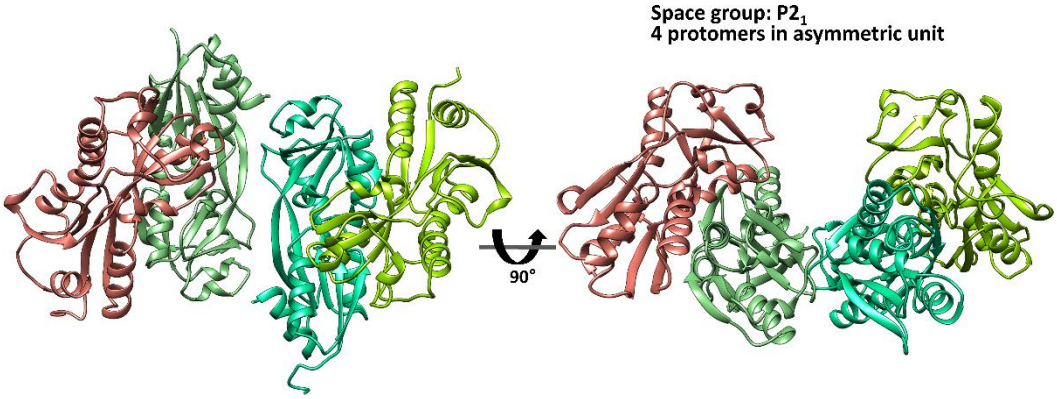

Figure 4. Overall structure of RipR RD.

The asymmetric unit contained four closely interacting protomers (pink, palegreen, cyan, and lightgreen), indicating two homodimeric assemblies of the RipR RD, similar to typical LTTR RDs

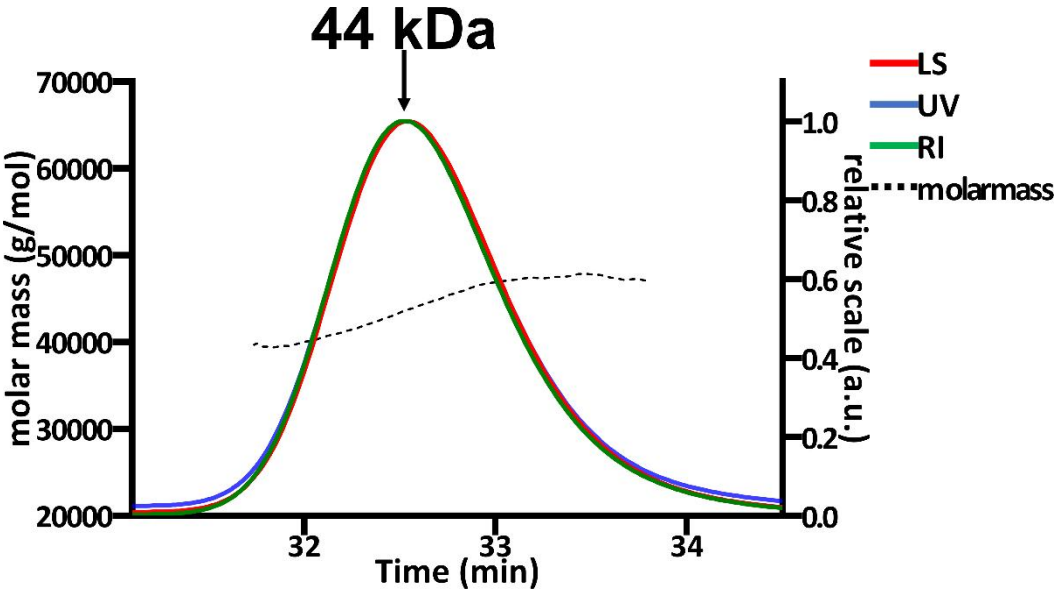

Figure 5. SEC-MALS of RipR RD.

Molecular size of the purified RipR RD protein. Primary y-axis, molar mass determined using multiangle light scattering (MALS; black dotted line); secondary y-axis, protein concentration, assessed by measuring the light scattering (LS; red), the absorbance at 280 nm (UV; blue), and the refractive index (RI; green). x-axis, elution time from size exclusion chromatography. The estimated molecular mass of the purified RipR RD is indicated above the peak.

3.3. Structural comparison to homolog *Acinetobacter balylyi* BenM RD

Similar to typical LTTR RDs, the RipR RD is further divided into the two subdomains RD-I and RD-II. RD-I from one protomer interacts with RD-II from the other protomer in the homodimeric arrangement (Fig. 3). The RD of the benzoate and cis-cis-muconate-responsive LTTR BenM was discovered as the top structural ortholog of RipR RD using the FoldSeek server (rmsd 1.536 Å; Table 2), which is a specialized program to search the structural homologs by sensitive comparisons of large structure sets (van Kempen *et al.*, 2022). The structural superposition on the ligand-bound structures of the BenM RD suggested the putative ligand binding site of RipR RD in the space between the two subdomains RD-I and RD-II (Fig. 6). Our RipR RD structure seemed to be a ligand-free structure, since no extra electron density map was found in the putative ligand binding pocket of RipR RD.

The putative ligand-binding sites of RipR RD were lined with Ser100, Arg148, and Leu202 (Fig. 6), which are mostly conserved among the RipR homologs and BenM (Craven *et al.*, 2009). In particular, the Arg residue corresponding to Arg148 makes the ionic interaction with the carboxylic acid of the bound cis-cis-muconate in the BenM RD (PDB code: 2F7A; Fig. 6).

Thus, these findings suggest that the cognate ligand of the RipR RD contains carboxylic acid moieties similar to the BenM RD.

Table 2. Results of a Foldseek search with the RipR structure

PDB ID	score	E-values	Sequence identity (%)	Gene ID	Description	Oligomer state
2H9B	787	4.292e-20	25.4	BenM from *Acinetobacter baylyi* ADP1 (R156H/T157S)	LysR-type transcriptional regulator	Homodimer
2F78	775	9.231e-20	25.7	BenM with its effector benzoate from *Acinetobacter baylyi*	LysR-type transcriptional regulator	Homodimer
2F7A	772	1.118e-19	25.7	BenM with its effector cis, cis-muconate from *Acinetobacter baylyi*	LysR-type transcriptional regulator	Homodimer
2H99	769	1.354e-19	25.7	BenM from *Acinetobacter baylyi* ADP1 (R156H, T157S)	LysR-type transcriptional regulator	Homodimer
2F97	764	1.863e-19	25.7	BenM from *Acinetobacter baylyi* ADP1 (high pH)	LysR-type transcriptional regulator	Homodimer
2F6G	755	3.308e-19	24.7	BenM from *Acinetobacter baylyi* ADP1	LysR-type transcriptional regulator	Homodimer
3GLB	753	3.758e-19	24.7	CatM from *Acinetobacter baylyi* ADP1 (R156H)	LysR-type transcriptional regulator	Homodimer

2H98	742	7.584e-19	25.7	CatM from *Acinetobacter baylyi* ADP1 (V158M)	LysR-type transcriptional regulator	Homodimer
3K1N	741	8.084e-19	25.7	BenM from *Acinetobacter baylyi* ADP1 (full-length)	LysR-type transcriptional regulator	Homodimer
3K1P	733	1.347e-18	24.6	BenM from *Acinetobacter baylyi* ADP1 (E226K) (full-length)	LysR-type transcriptional regulator	Homodimer
2F7C	727	1.975e-18	24.7	CatM with its effector cis, cis-muconate from *Acinetobacter baylyi*	LysR-type transcriptional regulator	Homodimer
1IXC	689	2.233e-17	21.6	CbnR from *Cupriavidus necator*	LysR-type transcriptional regulator	Homotetramer
6G1D	688	2.380e-17	24.1	OxyR from *Corynebacterium glutamicum*	LysR-type transcriptional regulator	Homotetramer
2HXR	680	3.966e-17	23	CynR from *Escherichia coli K-12*	Probable transcriptional regulator	Homodimer
5TED	678	4.505e-17	21.9	QuiR with shikimate from *Listeria monocytogenes* EGD-e	LysR-type transcriptional regulator	Homotrimer

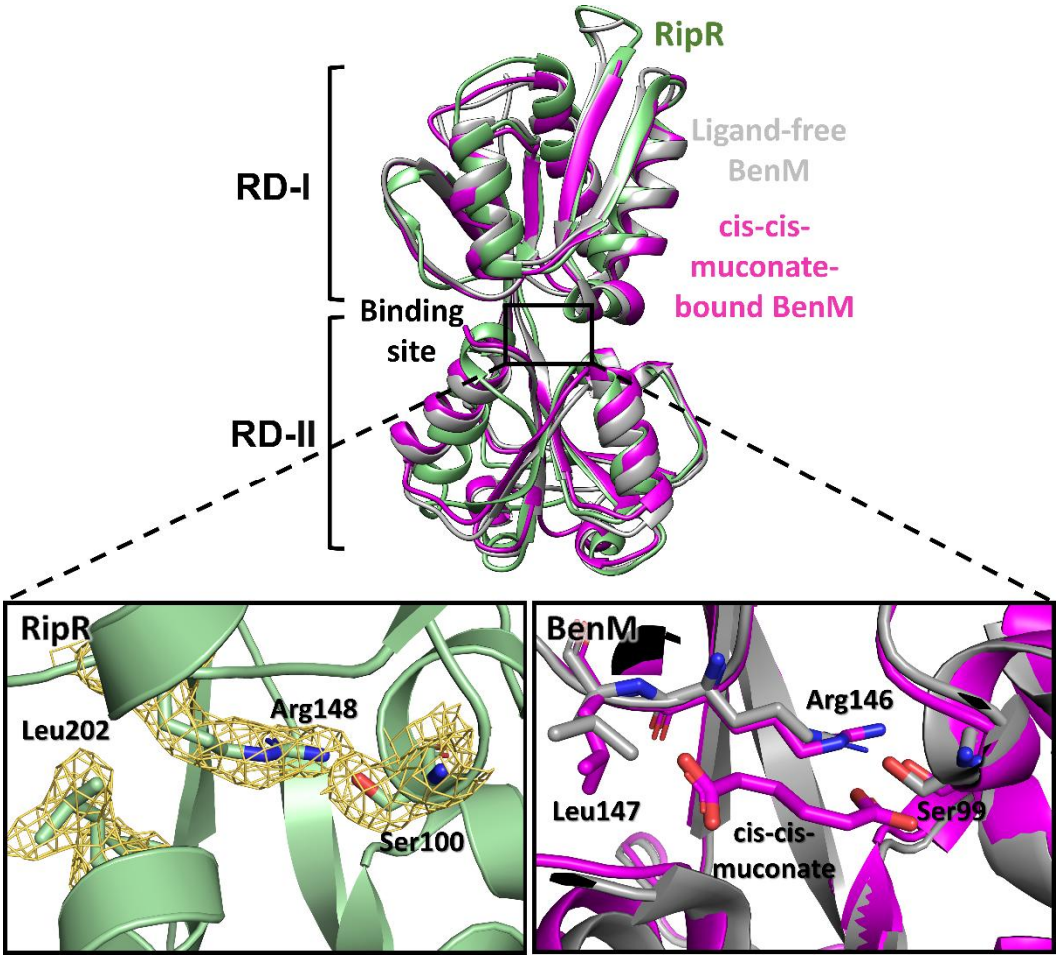

Figure 6. Structural superposition of RipR RD with its homolog BenM RD.

A protomer of the Rip RD (palegreen) was superposed on BenM RD from *Acinetobacter balylyi* (PDB code, 2F6G) representing the ligand-free form (rmsd = 1.536 Å) and on cis-cis-muconate-bound BenM RD (PDB code, 2F7A; rmsd = 1.571 Å). The red recangle indicates the putative ligand-binding site,

which is enlarged with the conserved residues involved in the ligand binding. The cis-cis-muconate is also depicted in stick representations in the bottom right. The electron density map of RipR is shown in yellow.

3.4. Isocitrate as the cognate ligand of RipR

To determine whether RipR of *S.* Typhimurium is responsive to the itaconic acid treatment, we treated *S.* Typhimurium with itaconic acid and investigated the transcription of the *ripCBA*, whose transcription is induced by RipR. The qRT-PCR results showed that the treatment of itaconic acid to the bacteria increased the expression levels of *ripCBA* by over 200-fold, confirming the role of RipR (Sasikaran *et al.*, 2014; Hersch and Navarre, 2020) (Fig. 7 and table 3). Since RipR plays a significant role in itaconic acid stress in *S.* Typhimurium, itaconic acid and its structural analogs were suggested to be the cognate ligands for RipR RD.

To seek the physiological ligand for RipR, we selected itaconic acid, together with its structural analogs, isocitrate, succinic acid, malic acid, oxaloacetate, and cis-aconitate, which are the di- or tricarboxylic acids found in the TCA cycle. We measured the binding affinities of the compounds to the RipR RD proteins using isothermal titration calorimetry (ITC) in 20 mM HEPES (pH 7.0). The ITC thermograms showed that isocitrate is strongly bound to the RipR RD with a submicromolar K_d value (0.31 μM) and a stoichiometry of 0.5 binding sites per RD monomer (Fig. 8). The heat from the binding of isocitrate was larger than the binding of 3-phenylpropionic acid

(Fig.8 and 19), which was unusually high and further indicated that many interactions were newly generated by isocitrate binding. In contrast, itaconic acid, succinic acid, malic acid, oxaloacetate and cis-aconitate did not give compelling results for binding to the RipR RD in the ITC experiments (Fig. 9).

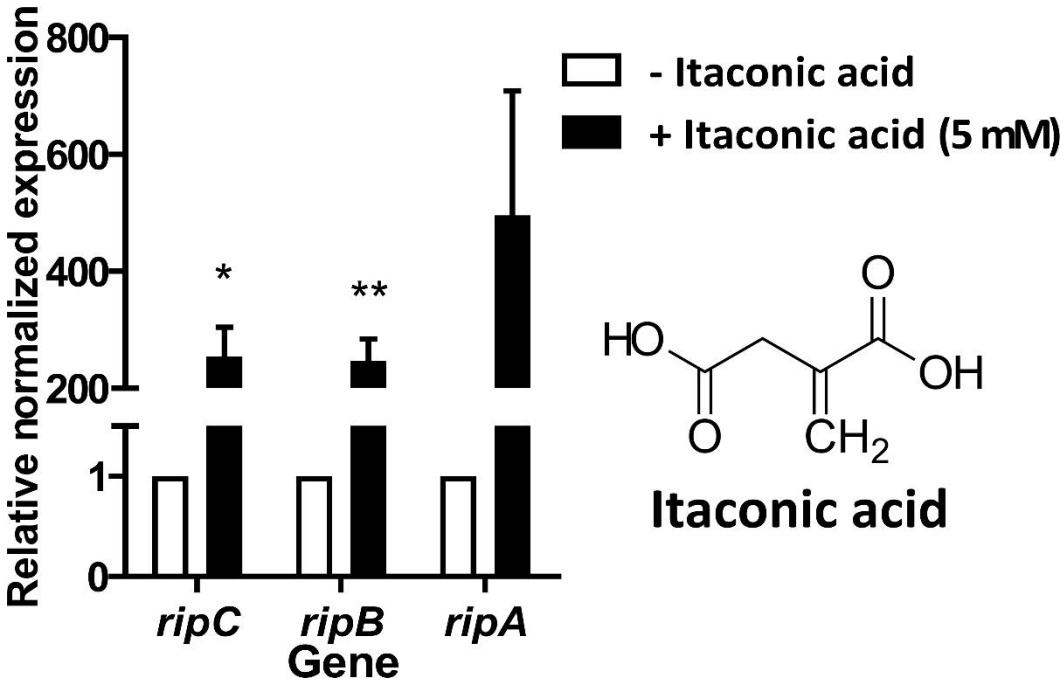

Figure 7. The quantitative real-time PCR (qRT-PCR) with itaconic acid treatment.

The transcriptional levels of *ripC*, *ripB*, and *ripA* in the *S.* Typhimurium SL1344 wild type were analyzed with quantitative real-time PCR (qRT–PCR). The strain was cultured in LB medium with or without 5 mM itaconic acid for 4 h. The expression value was normalized using samples cultured in LB broth without itaconic acid. Error bars represent SD values calculated from three replicate experiments, and the *P* value was calculated with Student's *t*-test. *$P < 0.05$; **$P < 0.01$.

Table 3. Primers used in this study.

Primer	Sequence (5′-3′)	Reference
qRT–PCR		
gyrB-RT-F	ATATCGGCGACACGGATGAC	This study
gyrB-RT-R	CCTTCTTCCGGGTGAATCCC	
ripC-RT-F	ATCCCGACCAAACTCATCGC	
ripC-RT-R	GCGAGTATCAGAACCAGCCA	
ripB-RT-F	GCCAGCAAAACGGAATGGAA	
ripB-RT-R	ACAGGCGTTTGCTGAGTACA	
ripA-RT-F	CCTCCAGCTTTGCTGAATGC	
ripA-RT-R	CCGGAACTCTCAATCCCCTG	

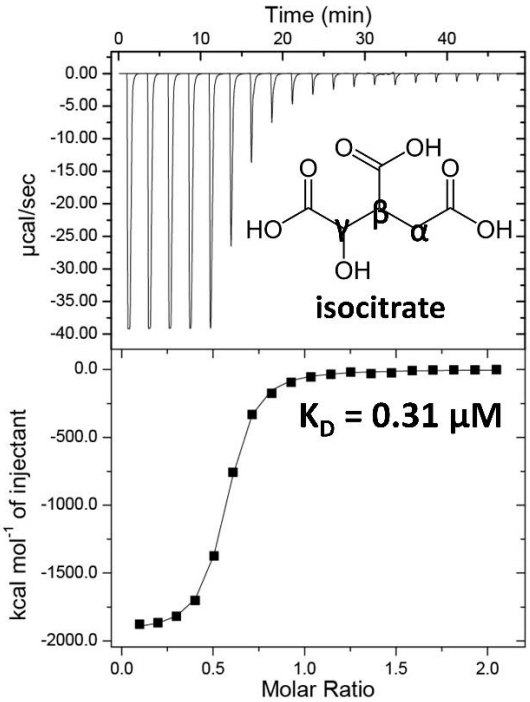

Figure 8. Isothermal titration calorimetry of isocitrate to RipR RD.

ITC graph for the titration of isocitrate to RipR RD. The ligand injection profile (raw data; top) and the calculated heat/enthalpy change for each ligand injection (bottom) are shown in the graph. The stoichiometry value (N) and KD of RipR RD with isocitrate were calculated as 0.5 sites and 0.31 µM, respectively.

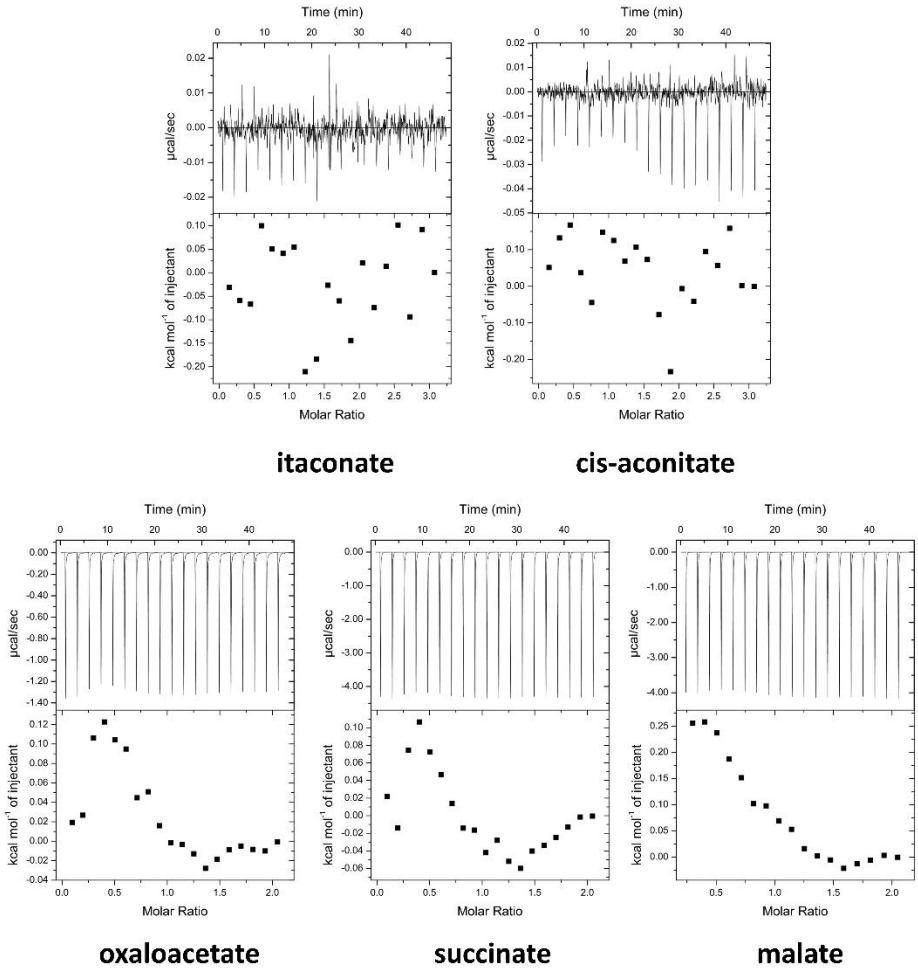

Figure 9. Isothermal titration calorimetry of structural analogs to RipR RD.

The ITC thermograms for the titration of the listed structural analogs in the tricarboxylic acid (TCA) cycle to RipR RD are displayed with the ligand injection profile (raw data; Top) and the calculated heat/enthalpy change for each ligand injection (Bottom). Each ligand is mentioned below the ITC graph.

3.5. Conformational change of RipR upon isocitrate binding by MD simulation

To further investigate isocitrate binding in the RipR RD, we attempted to solve the complex structure with isocitrate. Unfortunately, isocitrate seemed to hamper the co-crystallization of the protein and did not allow binding by soaking into the ligand-free crystals. We instead docked an isocitrate molecule on the putative ligand binding site of the RipR RD *in silico* by AutoDock Vina in PyRx (Dallakyan and Olson, 2015) (Fig. 10). The Gromacs program further minimized the energy of the docked structure, which depicted the isocitrate-bound ligand binding site (Fig. 11). The isocitrate molecule interacts with the side-chains of Glu127, Ile200, Thr98, Ala99, Ser100, Arg148, and Pro226 on the solvent-accessible ligand binding pocket of RipR RD in the docked structure (Fig. 12). In particular, Arg148 makes ionic interactions with a carboxylic acid moiety of isocitrate, as predicted by structural comparison to the cis-cis-muconate-bound BenM structure (Fig. 14 and 6). When the *in-silico* docking model was compared with the ligand-free crystal structure, substantial structural changes were not observed, which was not surprising because the AutoDock Vina and the energy minimization function in Gromacs did not allow a large conformational change of the receptor proteins (Fig. 10).

When we compared the elution volumes of the RipR RD in the buffer with and without isocitrate in the size exclusion chromatography, isocitrate increased the elution volume of the RipR RD (Fig. 13). These findings indicate that isocitrate binding makes the conformation of RipR RD more compact, as observed in many ligand-bound LTTR RDs. To analyze the structural change of the RipR RD dimer upon isocitrate binding, we performed the molecular dynamics (MD) simulation with the docked structure using the Gromacs program, which is widely used in molecular dynamics for biomolecules (Pronk *et al.*, 2013). The molecular motions of the protein and the ligand were largely stopped in 200 ns during the MD simulation process. According to the MD simulation result, the isocitrate molecule in a subunit (chain B) was moved into the interior of RD-II by 8 Å (Fig. 15), while the isocitrate molecule in the other subunit (chain A) of the RD dimer remained in the solvent-accessible ligand-binding pocket. A large rotational motion was observed in the chain B subunit when the chain A subunit was superposed as the reference, which may explain the high released heat upon isocitrate binding in the ITC experiments. The rotational motion resulted in a 9.7 Å movement of the N-terminal residue of the RD (Val92) in the MD simulation, which is connected to the DBD in the full-length model of RipR (Fig. 15). These findings suggest

that isocitrate binding to the RD domains induces the transition from the inactive conformation to the active conformation by the movement of the DBDs in the tetrameric assembly of full-length RipR.

We analyzed the MD simulation results focusing on how the changes in the isocitrate binding mode resulted in the conformational change of the RD domain. The α and γ-carboxylic groups and the hydroxyl group of isocitrate mediate the interaction between RD-I and RD-II. The α carboxylic acid group of isocitrate (pKa ~7.0) formed hydrogen bonds with the backbone or side-chains of RD-I Ala99 and Glu127, and the α-hydroxyl group of isocitrate with the carbonyl group of Pro226 in RD-II. The γ-carboxylic group formed hydrogen bonds with RD-I Ser100, Arg148 and RD-II Ile200 (Fig. 14). However, the isocitrate-mediated RD-I and RD-II interactions were shifted in the 200 ns structure, resulting in a rotational movement of the protomers in the dimeric assembly. The angle between one protomer and the other protomer of the isocitrate-bound RipR RD dimer was decreased by ~22° compared to the starting structure at 0 ns (Fig. 15). The carboxylic group at the α position makes interactions with Pro226 and Ile228 only in RD-II, and the γ-carboxylic group interacts with Leu202 of RD-II with the ionic interaction between the β-carboxylic group of isocitrate and Ser100 and Arg148 in RD-I (Fig. 14). The

distance of RD-I and RD-II at the ligand binding site (10.6 Å between RD-I Ser100 and RD-II Pro226 Cα atoms) at 0 ns was decreased at the final structure at 200 ns (9.6 Å between RD-I Ser100 and RD-II Pro226 Cα atoms), representing a typical ligand-dependent closing motion of the RDs (Fig. 16).

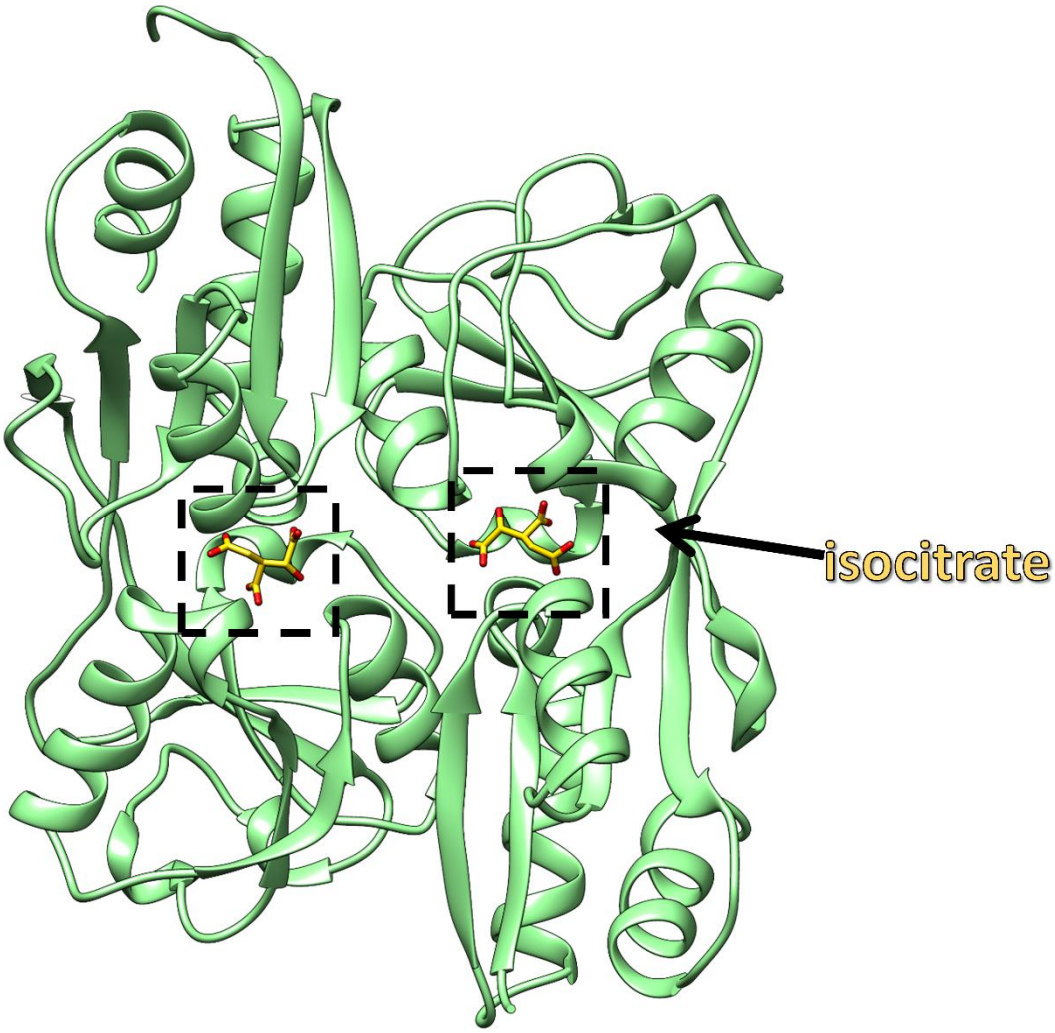

Figure 10. The docked structure of isocitrate on the ligand-free RipR RD.

Isocitrate molecules (yellow sticks) were first docked on the ligand-free RipR RD structure (gray ribbon) we determined in this study with PyRx.

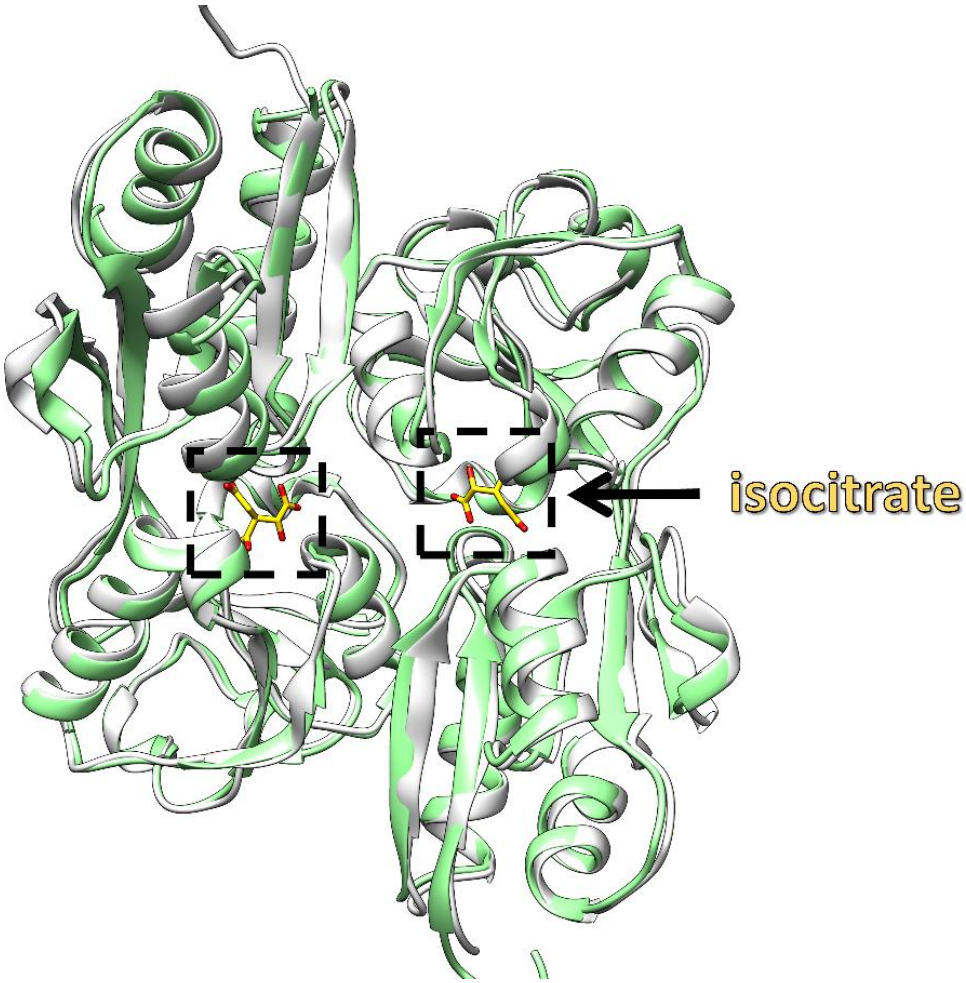

Figure 11. The Gromacs-refined structure of isocitrate on the ligand-free RipR RD.

The docked structure was further refined by the energy minimization and equilibrium procedures in the MD simulation program Gromacs (palegreen ribbon). The rmsd value between the docked structure and Grmoacs-refined structure is 0.831 Å.

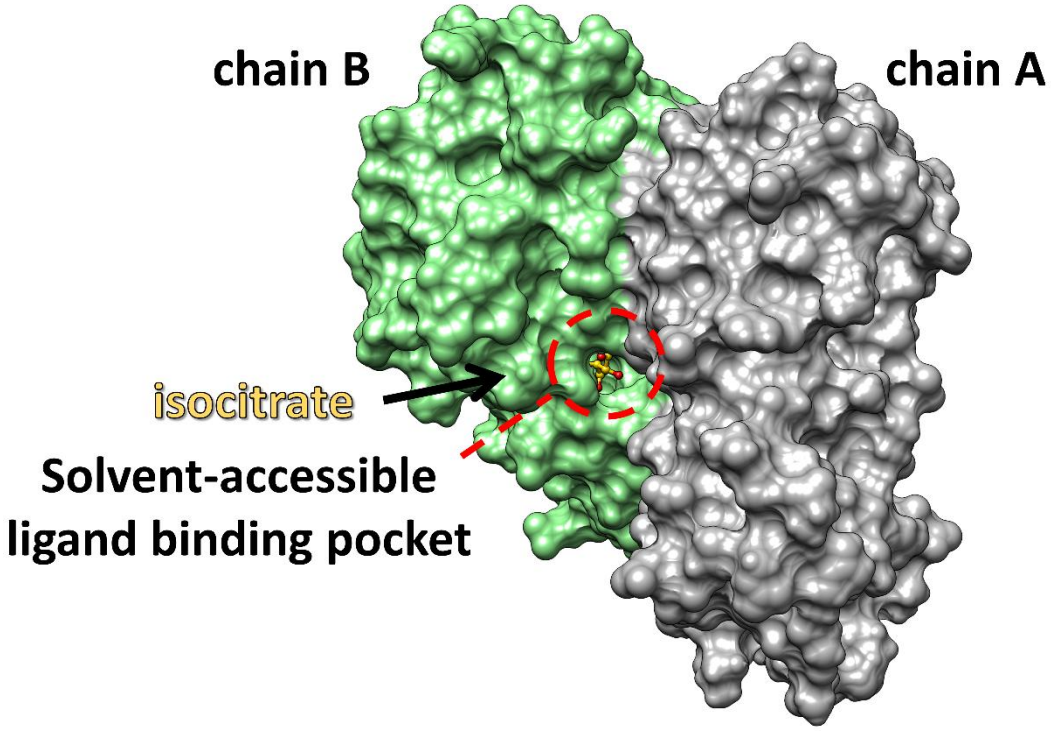

Figure 12. The surface representations of the Gromacs-refined complex structure.

The surface representations of the Gromacs-refined complex structure. Each protomer is colored differently, and the bound isocitrate is shown as the yellow sticks. Note that the bound isocitrate is accessible from the external solvent.

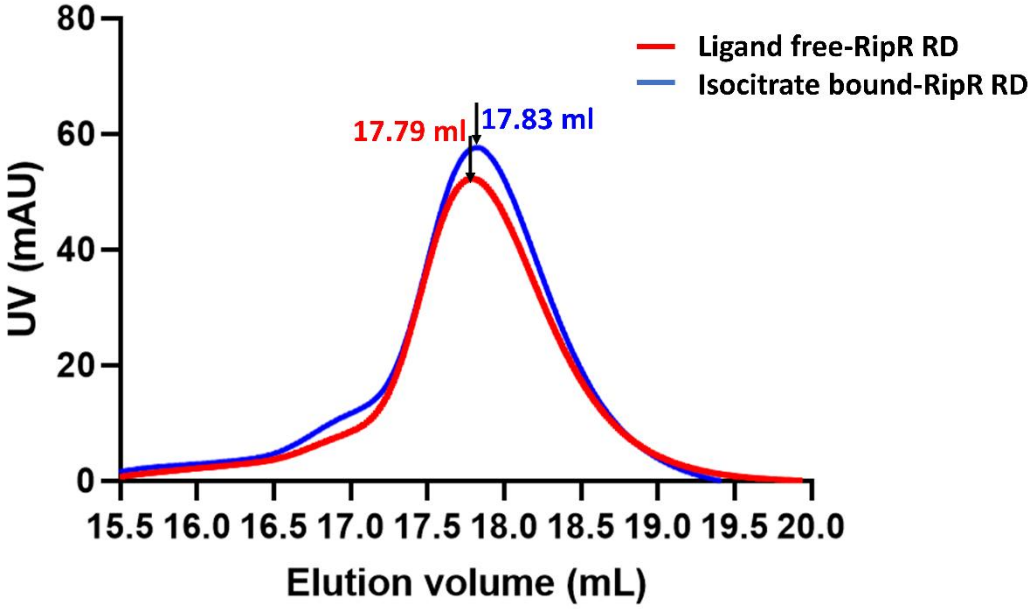

Figure 13. Comparisons of size exclusion chromatography (SEC) elution profiles between the ligand-free RipR and isocitrate-bound RipR.

The ligand-free RipR and isocitrate-bound RipR (165 μM) were injected on a Superdex 200 increase 10/300 GL column for profile comparison. Each elution volume of the main peak is indicated by a black arrow. The left y axis represents the absorbance at 280 nm and the x axis represents the elution volume. The scales for profiles in each graph are adjusted to be identical. The experiments were performed in triplicate.

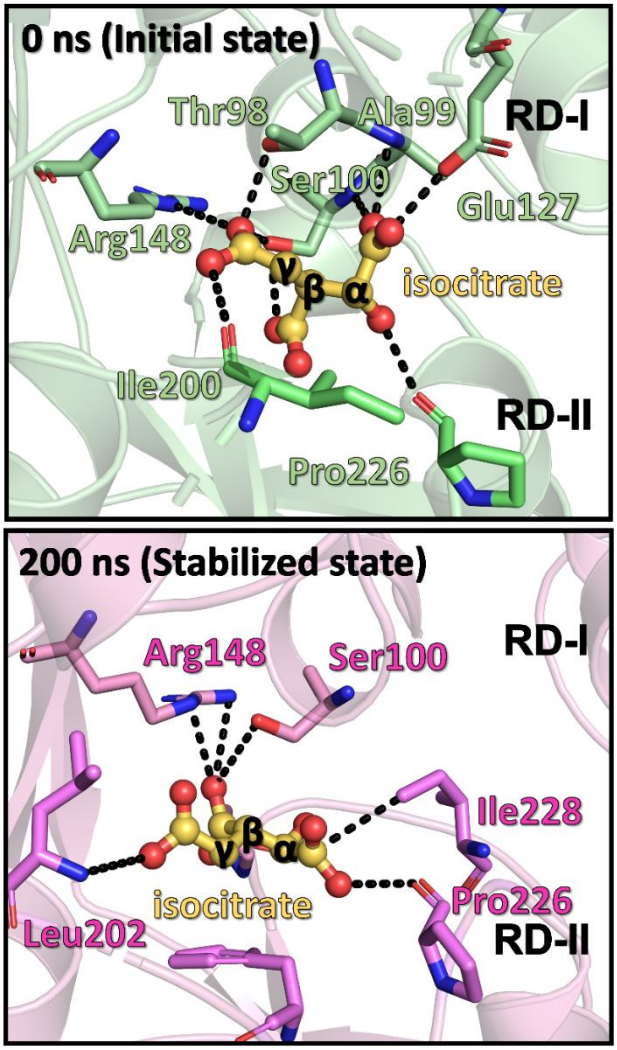

Figure 14. The ligand binding site between 0 ns (initial state structure) and 200 ns (stabilized state structure) of the RipR RD.

A close-up view of the ligand binding site. The residues surrounding the isocitrate are shown as a stick model, and the structures of RipR RD are shown as a cartoon model. The RD-I, and RD-II of RipR RD are indicated.

Critical residues are shown separately with observations from the same direction and same scale. Left: isocitrate-docking structure of the RipR RD, palegreen (RD-I) and green (RD-II). Right: 200 ns MD simulation structure of the RipR RD, lightpink (RD-I) and light purple (RD-II). The residues are shown as sticks. The isocitrate in the RipR RD is shown as a yellow ball and stick. The interactions between residues and isocitrate molecules are represented with dotted lines.

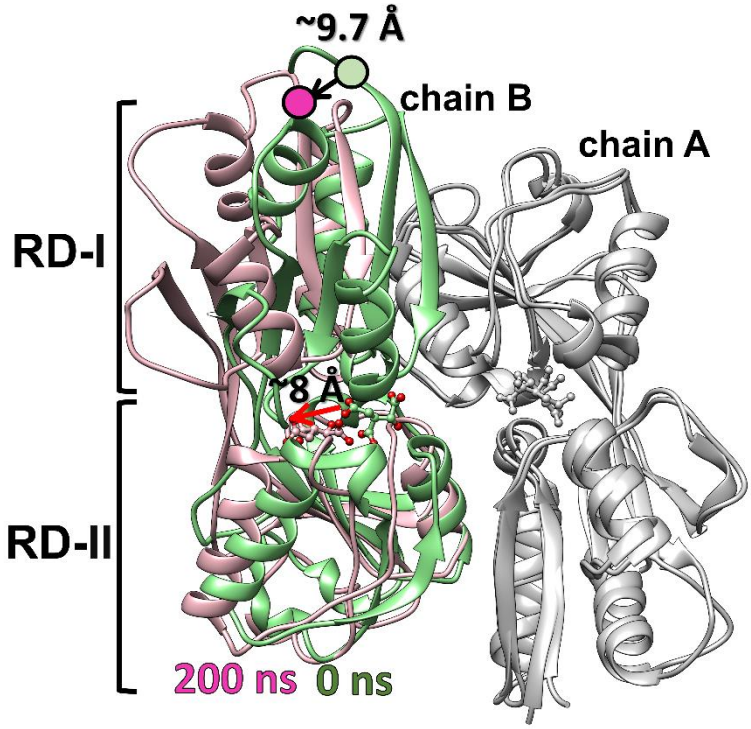
~9.7 Å
chain B
chain A
RD-I
~8 Å
RD-II
200 ns
0 ns

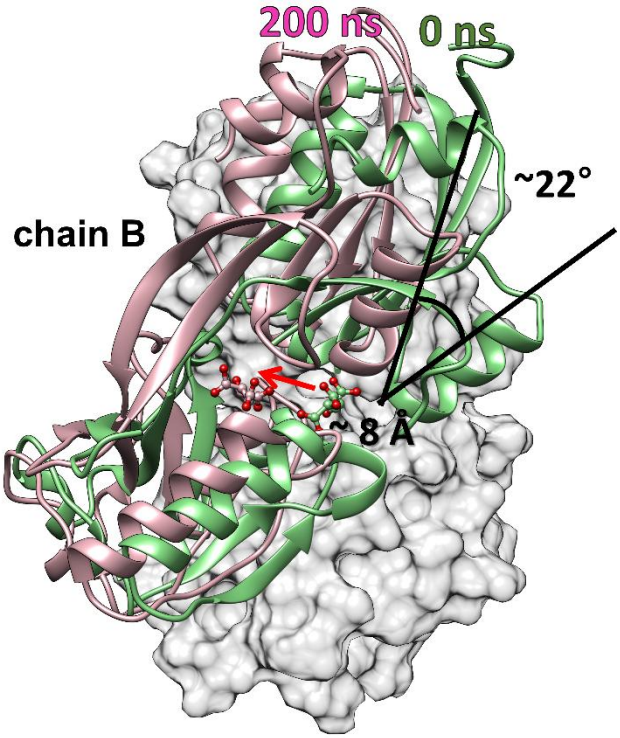
200 ns
0 ns
~22°
chain B
~ 8 Å

Figure 15. Structural superposition between chain B of 0 ns isocitrate-bound RipR RD and chain B of 200 ns isocitrate-bound RipR RD.

Structural superposition between chain B of 0 ns isocitrate-bound RipR RD (palegreen) and chain B of 200 ns isocitrate-bound RipR RD (lightpink). The length of the movements of the DBD connection points and the isocitrate are shown as arrows with each value (circle; DBD connection points, black arrow; DBD connection movement, red arrow; isocitrate movement). Each chain A in both dimers is colored gray, and chain B of the 0 ns isocitrate-bound dimer and chain B of the 200 ns isocitrate-bound dimer are colored palegreen and lightpink, respectively. (left) The angle (~22º) between chain B in the 0 ns isocitrate-bound RipR RD (palegreen) and chain B in the 200 ns isocitrate-bound RipR RD (pink) is shown as black lines with a value. Each chain A in both dimers is colored gray with surface representations.

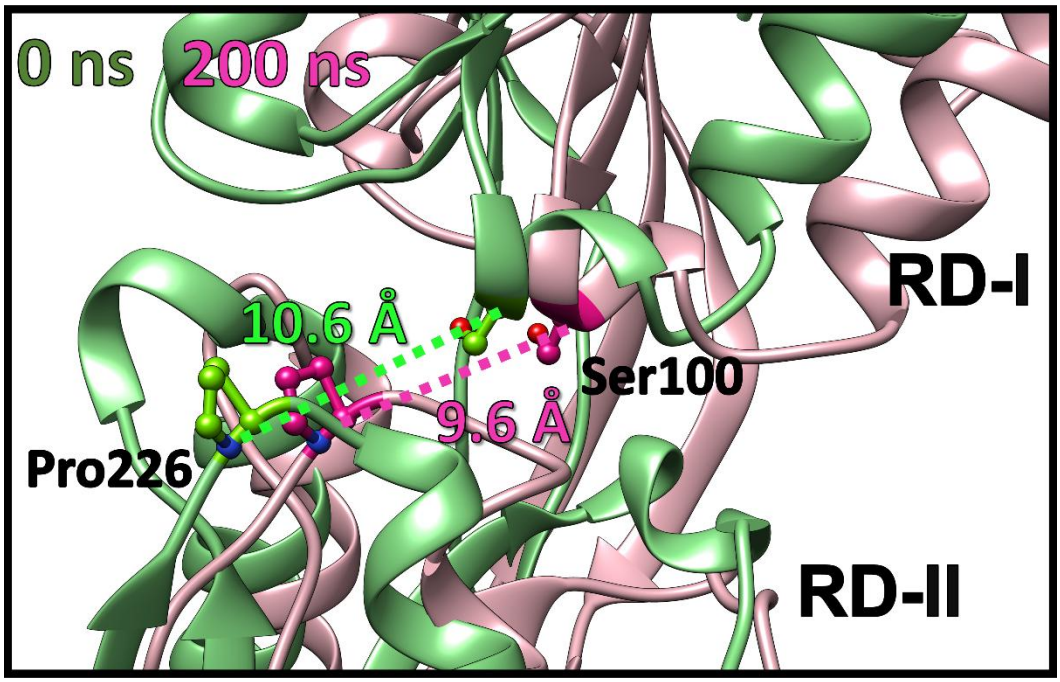

Figure 16. A close-up view of RD-I and RD-II at the ligand binding site in residues Ser100 and Pro226.

A close-up view of RD-I and RD-II at the ligand binding site in residues Ser100 and Pro226. The distances of the 0 ns and 200 ns structures are shown as dotted lines colored in green and pink, respectively. The residues are drawn in ball and stick format with values shown.

3.6. Sequence alignment with homolog Escherichia coli HcaR

A BLAST search revealed that the *E. coli* HcaR gene has the highest sequence similarity (54.4%) to *S.* Typhimurium RipR. In *E. coli*, the LTTR HcaR recognizes hydroxycarboxylic acids, such as 3-phenylpropionic acid and its derivatives, regulating the genes of HcaA1, HcaA2, HcaC, HcaD and HcaB (Burlingame and Chapman, 1983; Diaz *et al.*, 1998; Manso *et al.*, 2009) (Fig. 3 and 17). Although HcaR and RipR show different physiological responses, RipR and HcaR have the carboxylic acid group as the common moiety of their cognate ligands (Manso *et al.*, 2009). Moreover, the Alphafold 2-predicted HcaR RD structure showed a high structural similarity to RipR RD, including the ligand-binding site-lining residues (Fig. 17 and 18). Thus, we tested whether 3-phenylpropionic acid is bound to RipR. The ITC experiment showed that the binding of 3-phenylpropionic acid to RipR RD (K_d value = 5.22 μM) released less heat than those from the isocitrate binding (Fig. 19 and 8). These results suggested that 3-phenylpropionic acid binds to RipR RD with a less extensive structural change upon ligand binding than isocitrate.

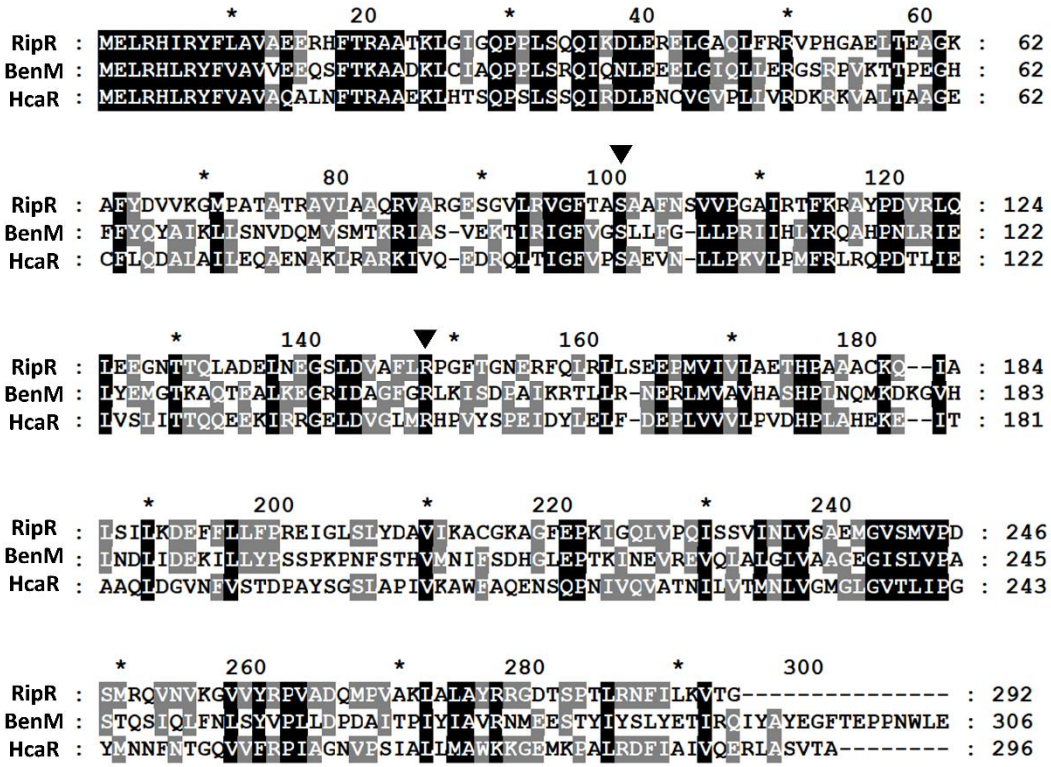

Figure 17. The sequence aligment of RipR and its homologs.

Sequences of RipR are aligned to its homologs: BenM, *Acinetobacter balylyi*; HcaR, *Escherichia coli*, by ClustalX (Thompson *et al.*, 1997). The conserved residues for recognition of the ligands are indicated by triangles.

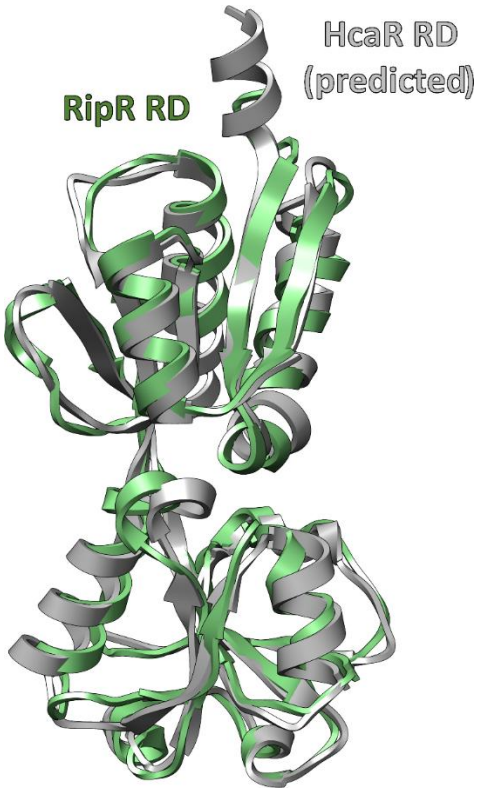

Figure 18. Structural superposition of RipR RD and Alphafold 2-predicted HcaR RD.

The *E. coli* HcaR RD structure was predicted by Alphafold 2 using residues 80-296. For structural comparison, the predicted HcaR RD structure (gray) is superposed on the ligand-free RipR RD (palegreen) (rmsd = 1.444 Å).

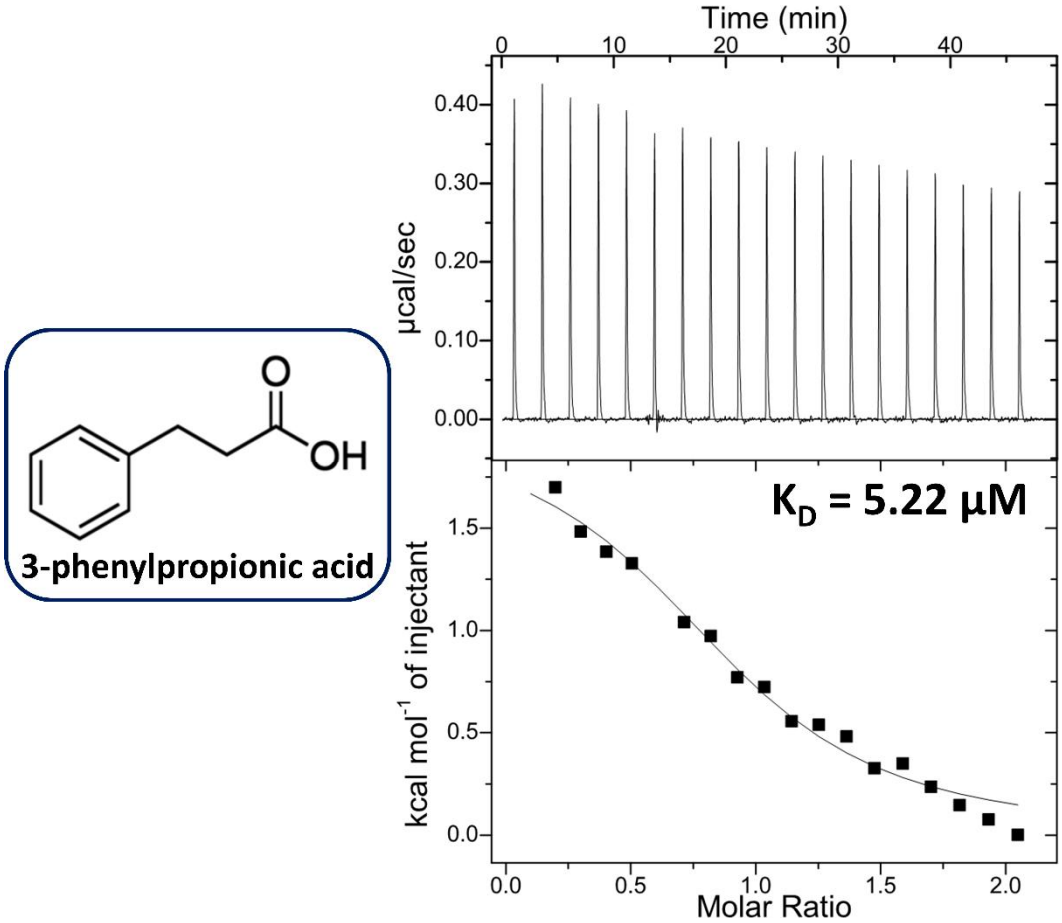

Figure 19. Isothermal titration calorimetry of 3-phenylpropionic acid to RipR RD.

The ligand titration profile (raw data; top) and the calculated heat/enthalpy change for each titrataion (bottom) are shown in the graph. The stoichiometry value (N) and K_D of RipR RD with 3-phenylpropionic acid were calculated as one site and 5.22 µM, respectively.

3.7. Overexpression and purification of RipR in comlex with 3-phenylpropionic acid

To gain mechanistic insights on RipR RD in complex with 3-phenylpropionic acid from its 3D structures, We expressed the RD (residues 87-292) of RipR from *S. enterica* serovar Typhimurium (*S.* Typhimurium) in the *Escherichia coli* expression system. The purified protein was crystallized in the space group of $P\ 3_1 2_1$, and its crystal structure was determined at 2.8 Å resolution by the molecular replacement method (Fig. 20). The search model for the molecular replacement was RipR RD wildtype.

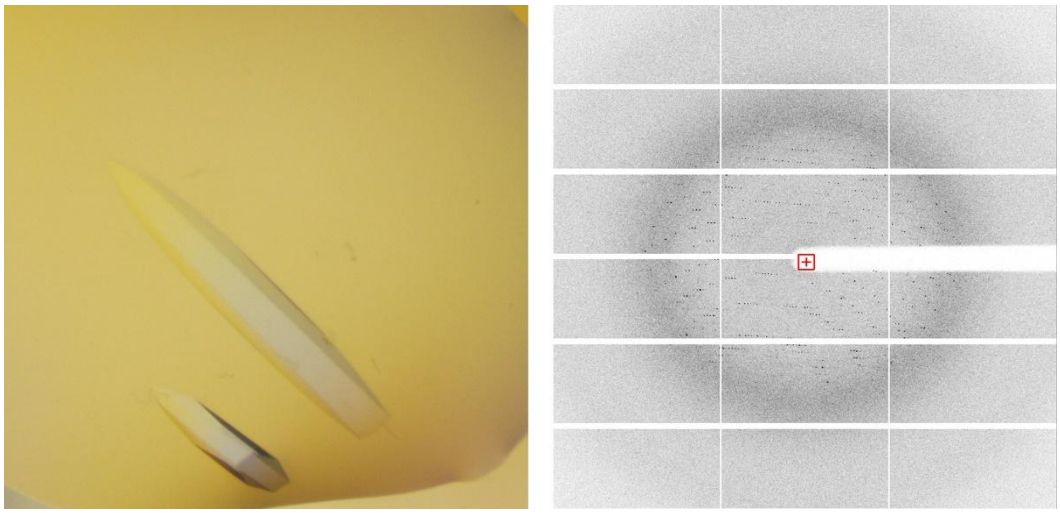

Figure 20. Crystals and X-ray diffraction image of RipR RD with 3-phenylpropionic acid.

3.8. Structural determination and overall structure of RipR RD in complex with 3-phenylpropionic acid

3-phenylpropionic acid was bound in the ligand binding site between the intersubdomain space (Fig. 21). The carboxylic moiety of 3-phenylpropionic acid was near residues Ser100 and Arg148, and the phenyl ring was surrounded by Leu202 and Leu204 (Fig. 22). Comparing the 3-phenylpropionic acid-bound structure of RipR and the benzoic acid-bound structure of BenM, the positions of the phenyl ring moiety and carboxylic moiety were similar The phenyl ring moiety was captured by Leu202 and the carboxylic moiety interacted with Ser100 and Arg148 (Fig. 23). However, we found that the binding of 3-phenylpropionic acid did not substantially change the conformation of the RipR RD structure when it was superposed on the ligand-free structure (Fig. 24). These findings suggest that 3-phenylpropionic acid interfered with the RipR function in itaconic acid resistance, but did not activate RipR function.

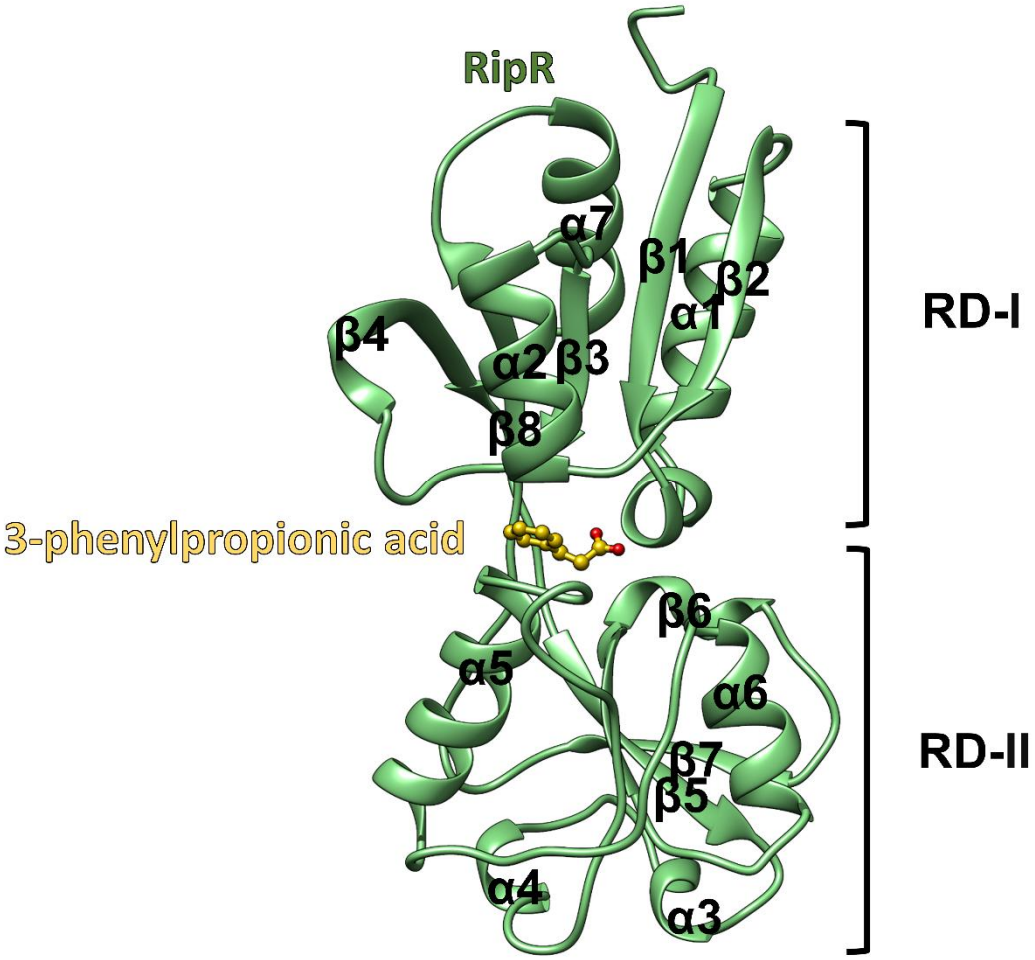

Figure 21. Overall structure of RipR RD in complex with 3-phenylpropionic acid.

Structural superposition between 3-phenylpropionic acid-bound RipR RD (palegreen) and ligand-free RipR RD (gray). (rmsd = 0.603 Å)

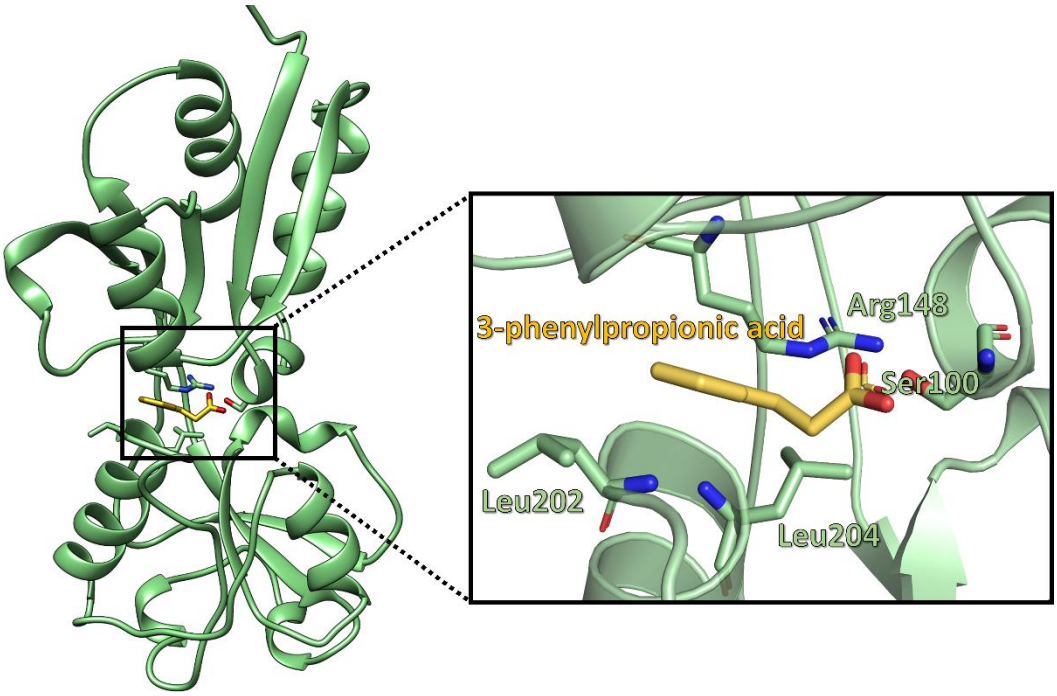

Figure 22. A close-up view of 3-phenylpropionic acid-bound RipR ligand binding site.

The 3-phenylpropionic acid is shown as a stick (yellow) and the interacting residues are represented as sticks. The black rectangle indicates the interacting residues for 3-phenylpropionic acid and RipR RD in a close-up view.

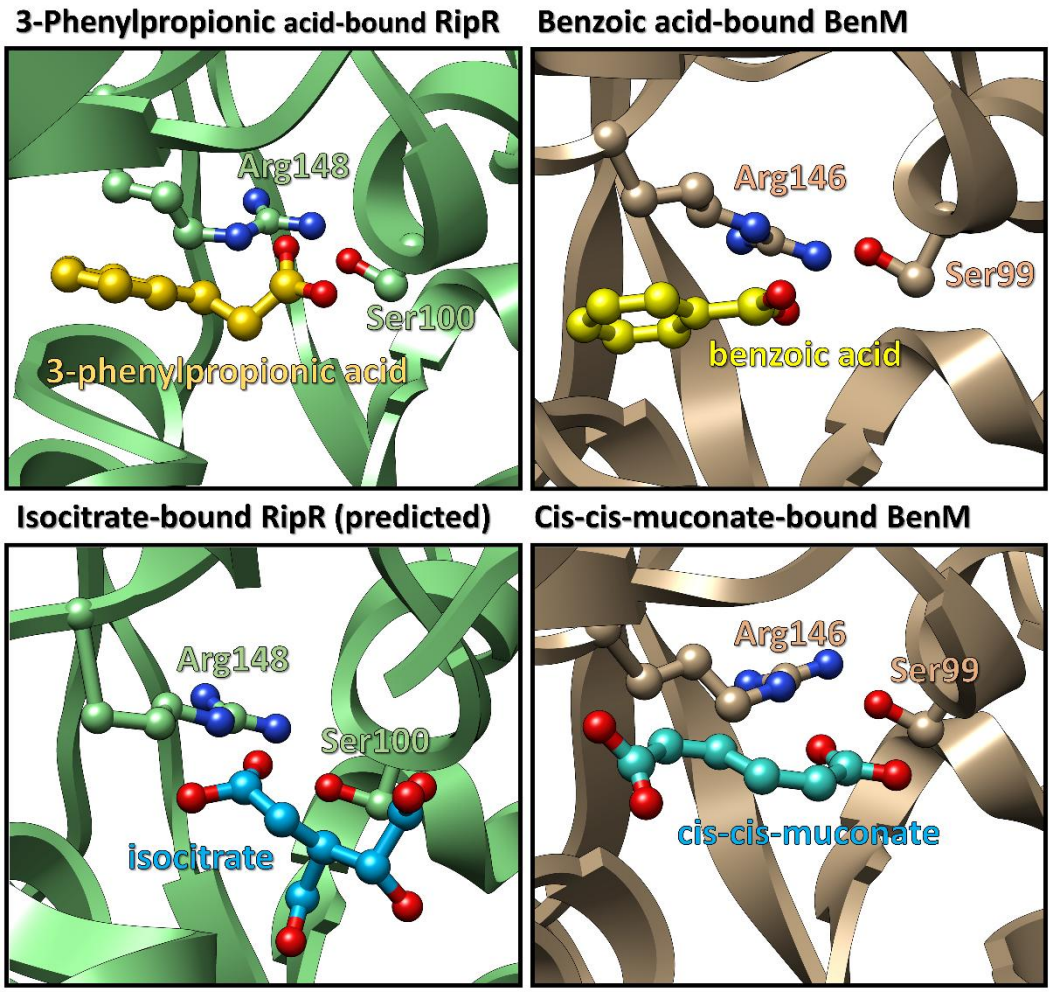

Figure 23. The roles of Arg148 and Ser100 or their corresponding residues of RipR RD and BenM RD in recognition of the carboxylic group of the ligands.

The complex structures are shown as labeled above the figure. Arg148 and Ser100 of RipR and Arg146 and Ser99 of BenM are shown as stick

representations. The bound ligands are shown as the stick representations: 3-phenylpropionyl acid (3-PP; gold), benzoic acid (yellow), isocitrate (blue), and cis-cis-muconate (cyan). Note that the isocitrate-bound RipR structure was predicted by PyRx and Gromacs (see main text), while the others were determined experimentally.

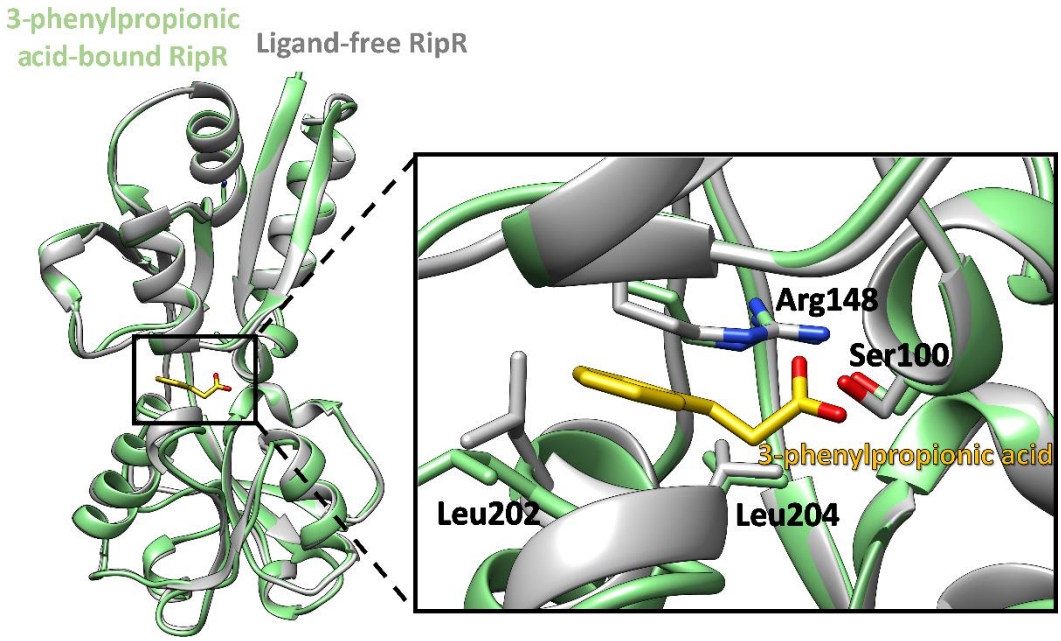

Figure 24. Overall structure comparison of ligand-free RipR RD with the RipR RD with 3-phenylpropionic acid complex.

Structural superposition between 3-phenylpropionic acid-bound RipR RD (palegreen) and ligand-free RipR RD (gray). (rmsd = 0.603 Å) The 3-phenylpropionic acid is shown as a stick (yellow) and the interacting residues are represented as sticks. The black rectangle indicates the interacting residues for 3-phenylpropionic acid and RipR RD in a close-up view.

3.9. 3-phenylpropionic acid as a RipR inhibitor

To test whether the inhibitory function of 3-phenylpropionic acid against itaconic acid stress occurred, we cultured *S*. Typhimurium in the presence of itaconic acid and/or 3-phenylpropionic acid. Bacterial growth was not significantly inhibited at concentrations below 1 mM itaconic acid in the absence of 3-phenylpropionic acid (Fig. 25). Interestingly, 3-phenylpropionic acid alone slightly increased the growth rate of the bacteria without itaconic acid treatment (Fig. 25). Notably, the cotreatment of 10 mM itaconic acid and 0.5 or 1 mM 3-phenylpropionic acid completely shut down the bacterial growth (Fig. 25). We further investigated the transcriptional levels of the *ripCBA* by 3-phenylpropionic acid treatment of the bacteria in the presence of 5 mM itaconate in the growth media. We found that the treatment of 1 mM 3-phenylpropionic acid to bacteria decreased the transcriptional levels of *ripCBA* by qRT-PCR (Fig. 26). The results demonstrated that 3-phenylpropionic acid is an inhibitor of RipR that reduces the transcriptional activity of RipR in response to itaconic acid stress.

To further analyze how 3-phenylpropionic acid affects the binding of isocitrate to the RipR RD protein, we measured the binding affinity of isocitrate to the RipR RD protein in the presence of 3-phenylpropionic acid by

using the ITC. We performed the ITC experiment by adding 3-phenylpropionic acid to both sample cell containing the RipR RD protein and injection syringe containing 300 μM isocitrate. No apparent binding enthalpy of isocitrate to the RipR RD protein was detected (Fig. 27), in sharp contrast to the large binding enthalpy of isocitrate in the absence of 3-phenylpropionic acid (Fig. 8). Since the large binding enthalpy of isocitrate also imply the structural change of RipR RD, our findings suggest that 3-phenylpropionic acid inhibits both the isocitrate binding and the ligand-induced activation of RipR.

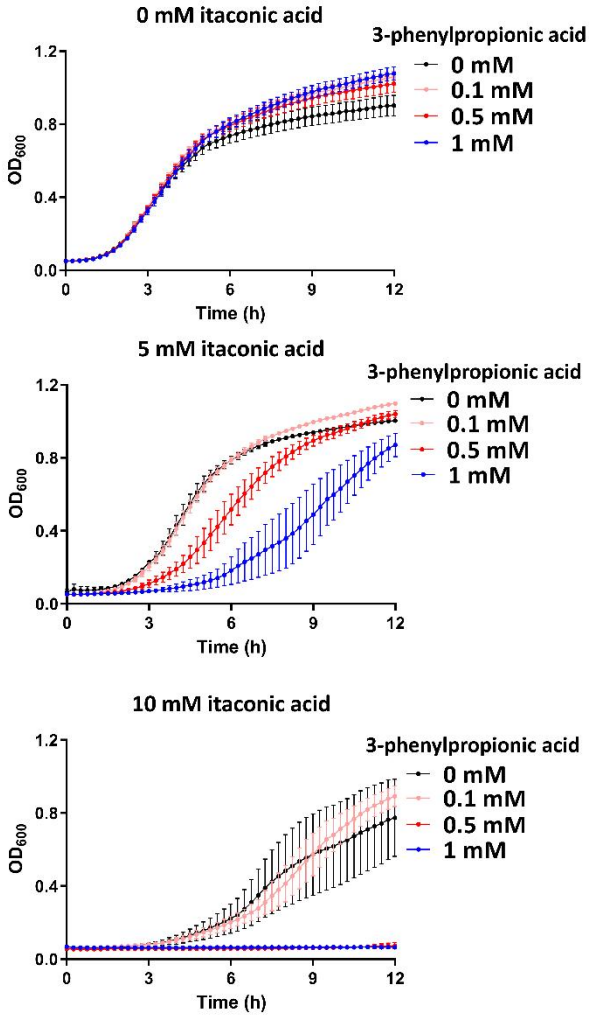

Figure 25. The bacterial growth in the presence of itaconic acid and/or 3-phenylpropionic acid.

Growth curves of wild-type *S.* Typhimurium SL1344 in LB medium with various concentrations (0, 0.1, 0.5, and 1 mM) of 3-phenylpropionic acid were measured by OD_{600}. The mean and SEM values were calculated from three replicate experiments.

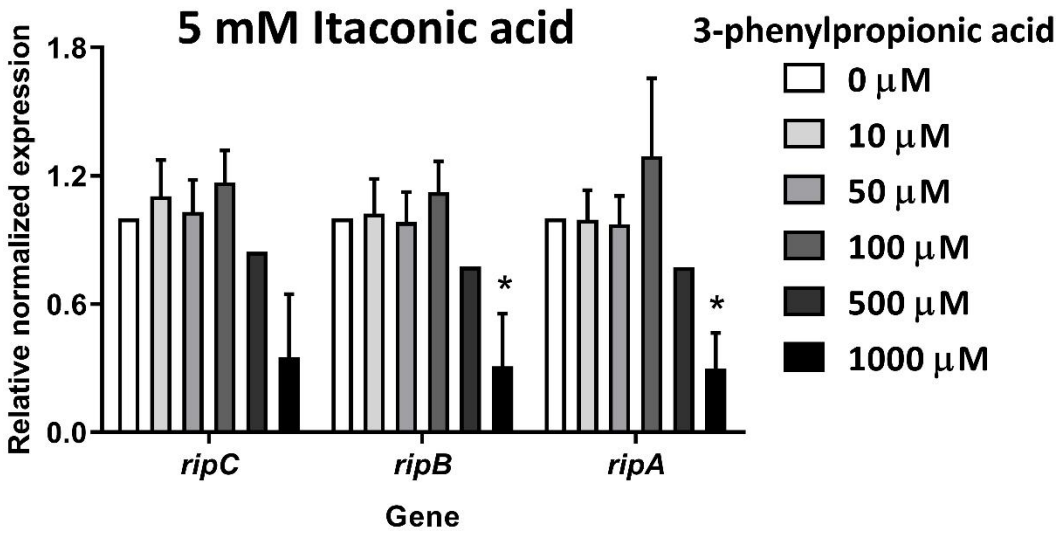

Figure 26. The quantitative real-time PCR (qRT-PCR) with itaconic acid at the various concentrations of 3-phenylpropionic acid.

The transcriptional levels of *ripC*, *ripB*, and *ripA* in the *S*. Typhimurium SL1344 were analyzed with quantitative real-time PCR (qRT-PCR). The strain was cultured in LB medium for 4 h with 5 mM itaconic acid at the indicated concentrations of 3-phenylpropionic acid. The expression values were normalized using samples cultured in LB medium containing 5 mM itaconic acid without 3-phenylpropionic acid. Error bars represent SD values calculated from three replicate experiments, and the *P* value was calculated with Student's *t*-test. $*P < 0.05$.

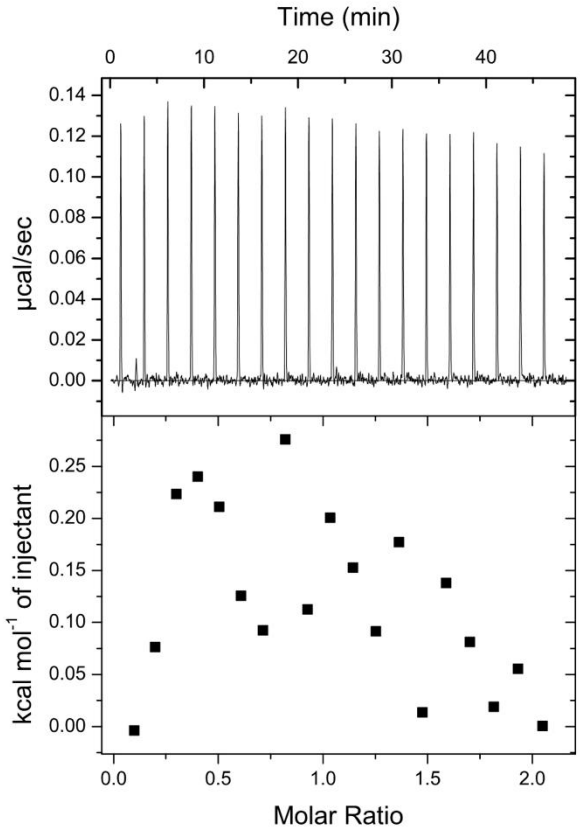

Figure 27. Isothermal titration calorimetry of the isocitrate to RipR RD in the presence of 3-phenylpropionic acid.

The ITC thermograms for the titration of the isocitrate to RipR RD in the presence of 3-phenylpropionic acid in both ligand and macromolecule are displayed with the ligand injection profile (raw data; Top) and the calculated heat/enthalpy for ligand injection (Bottom).

IV. Discussions

Itaconic acid exhibits antimicrobial activity by inhibiting isocitrate lyase, which is the crucial and first enzyme of the glyoxylate cycle by converting isocitrate into glyoxylate and succinic acid (McFadden and Purohit, 1977). The bacterial RipR saves the glyoxylate cycle from itaconic acid stress by inducing the bacterial itaconic acid-degradation enzyme (Hersch and Navarre, 2020). In this study, we determined the crystal structure of *Salmonella enterica* RipR RD in its dimeric form. We revealed that isocitrate was the strong ligand causing the structural change of the RipR RD into the active conformation by ITC and *in silico* simulation studies. We also found 3-phenylpropionic acid as an inhibitor of RipR at the molecular and the cellular levels.

Isocitrate is the compound at the branching point between the TCA cycle and glyoxylate cycle. Under carbon source-limiting conditions, isocitrate dehydrogenase in the TCA cycle is inhibited and isocitrate lyase in the glyoxylate cycle is instead activated (Cronan and Laporte, 2005). Since it is expected that the inhibition of isocitrate lyase by itaconic acid increases the

cellular isocitrate level, which is the substrate of isocitrate lyase in the glyoxylate cycle, the recognition of isocitrate by RipR is a reasonable response to cope with the abnormal metabolic situation caused by itaconic acid. Why does RipR recognize isocitrate, but not itaconic acid? We noted that itaconic acid has many structural analogs in its metabolites and does not have a distinguishing moiety to make a possible polar interaction with its receptor proteins. In contrast, isocitrate has structural features that can be specifically recognized by enzymes, such as isocitrate lyase and isocitrate dehydrogenase. Thus, we speculate that RipR has evolved to recognize isocitrate but not itaconic acid.

Since the glyoxylate cycle is central in the metabolism of pathogenic species including plants, bacteria, and fungi, isocitrate lyase is the current inhibition target for controlling diseases related to pathogens. Although the glyoxylate cycle is present in some animals, mammals including humans, do not perform the glyoxylate cycle (Lorenz and Fink, 2001). In this study, we discovered 3-phenylpropionic acid as a potential inhibitor of RipR action in *Salmonella* in the presence of itaconic acid. 3-Phenylpropionic acid belongs to the class of organic compounds known as phenylpropanoids (Diaz *et al.*, 1998). Furthermore, it is among the most ubiquitous aromatic-compound

catabolic systems (Burlingame and Chapman, 1983; Barnes *et al.*, 1997; Diaz *et al.*, 1998). 3-Phenylpropionic acid has been identified as a volatile constituent of grapes and has a wide variety of uses including applications in cosmetics, food additives (wine making, aging, storage), and pharmaceuticals to control contaminating bacteria (Api *et al.*, 2019). Thus, our study may add the role of 3-phenylpropionic acid in controlling *Salmonella* species in food by inhibiting normal bacterial metabolism by activating itaconic acid actions.

We next noted that the RipR RD structure shares the residues lining the putative ligand binding sites with many LTTR RDs, such as BenM and HcaR, whose functions are not directly related to the known function of RipR in the glyoxylate cycle. The sequence identity of RipR RD to RDs of BenM and HcaR (35.0% and 38.4%) is not high enough to consider them functional orthologs (Fig. 3). However, the lining residues that interact with the ligands are shared. These findings suggest that they have a common ancestral LTTR that could recognize carboxylic acids (Fig. 23).

In this study, we investigated the structure and ligand of RipR from *S.* Typhimurium, and the bacterial strategy for maintaining the homeostasis of their metabolic pathways from mammalian antimicrobial metabolites in terms of structural and evolutionary aspects. Furthermore, our findings suggest that

the natural compound 3-phenylpropionic acid may be a good inhibitor for restraining pathogenic bacteria (Fig. 28).

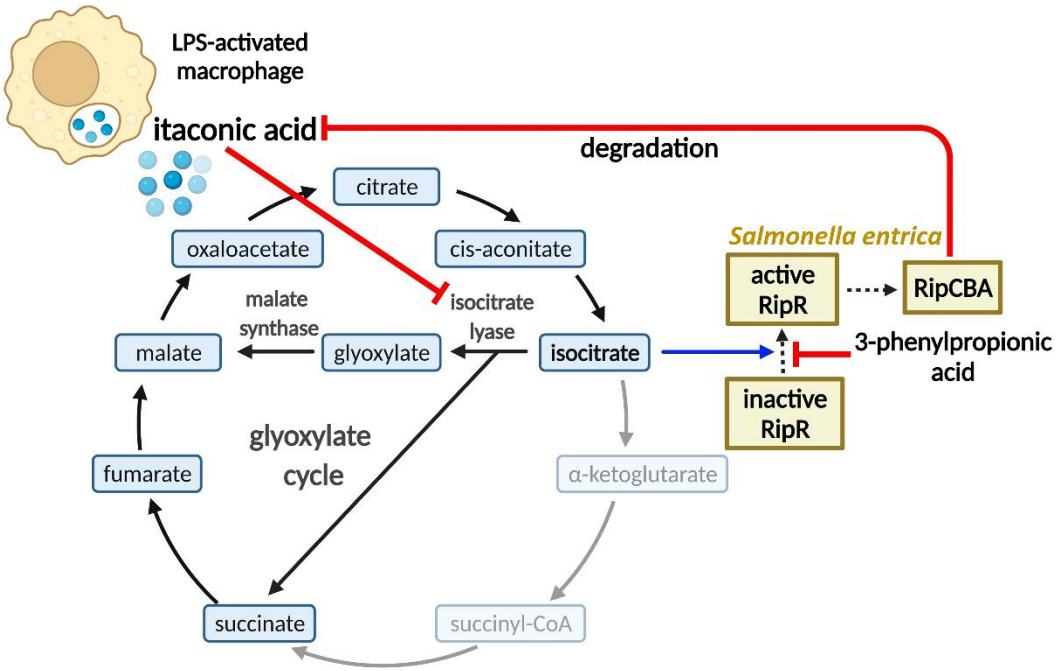

Figure 28. Proposed mechanisms of RipR in defense against itaconic acid stress.

Schematic diagram of the roles of the LTTRs (light yellow boxes) RipR and RipCBA. LPS-activated macrophages produce itaconic acid in their phagosomes. *Salmonella* employs the gloxylate cycle in the phagosome environment, and the function of isocitrate lyase in the glyoxylate cycle becomes critical for bacterial survival. Itaconic acid inhibits *Salmonella* isocitrate lyase, accumulating isocitrate in the bacterial cytosol in a competitive inhibitory manner. Bacterial RipR recognizes isocitrate and induces the expression of *ripCBA*, which decomposes the cellular itaconic acid

to resume the glyoxylate cycle to survive. The natural compound 3-phenylpropionic acid inhibits RipR function, which makes the bacteria vulnerable to itaconic acid stress. The black and gray arrows indicate the glyoxylate cycle and tricarboxylic acid cycle, respectively. The blue arrow indicates that RipR recognizes isocitrate as a ligand to induce the expression of RipCBA. The suppression of the activity is indicated by red lines. The activation of the activity is indicated by dotted lines.

V. References

Adams, P.D., Afonine, P.V., Bunkoczi, G., Chen, V.B., Davis, I.W., Echols, N., Headd, J.J., Hung, L.W., Kapral, G.J., Grosse-Kunstleve, R.W., McCoy, A.J., Moriarty, N.W., Oeffner, R., Read, R.J., Richardson, D.C., Richardson, J.S., Terwilliger, T.C., and Zwart, P.H. 2010. PHENIX: a comprehensive Python-based system for macromolecular structure solution. *Acta Crystallogr D Biol Crystallogr* **66**, 213-221.

Api, A.M., Belsito, D., Botelho, D., Bruze, M., Burton, G.A., Jr., Buschmann, J., Dagli, M.L., Date, M., Dekant, W., Deodhar, C., Francis, M., Fryer, A.D., Jones, L., Joshi, K., La Cava, S., Lapczynski, A., Liebler, D.C., O'Brien, D., Patel, A., Penning, T.M., Ritacco, G., Romine, J., Sadekar, N., Salvito, D., Schultz, T.W., Sipes, I.G., Sullivan, G., Thakkar, Y., Tokura, Y., and Tsang, S. 2019. RIFM fragrance ingredient safety assessment, 3-phenylpropionic acid, CAS Registry Number 501-52-0. *Food Chem Toxicol* **134 Suppl 1**, 110601.

Barnes, M.R., Duetz, W.A., and Williams, P.A. 1997. A 3-(3-hydroxyphenyl)propionic acid catabolic pathway in Rhodococcus globerulus PWD1: cloning and characterization of the hpp operon. *J Bacteriol* **179**, 6145-6153.

Basler, T., Jeckstadt, S., Valentin-Weigand, P., and Goethe, R. 2006. Mycobacterium paratuberculosis, Mycobacterium smegmatis, and lipopolysaccharide induce different transcriptional and post-transcriptional regulation of the IRG1 gene in murine macrophages. *J Leukoc Biol* **79**, 628-638.

Bintsis, T. 2017. Foodborne pathogens. *AIMS Microbiol* **3**, 529-563.

Burlingame, R., and Chapman, P.J. 1983. Catabolism of phenylpropionic acid and its 3-hydroxy derivative by Escherichia coli. *J Bacteriol* **155**, 113-121.

Chew, S.Y., Chee, W.J.Y., and Than, L.T.L. 2019. The glyoxylate cycle and alternative carbon metabolism as metabolic adaptation strategies of Candida glabrata: perspectives from Candida albicans and Saccharomyces cerevisiae. *Journal of Biomedical Science* **26**, 52.

Chew, S.Y., and Than, L.T.L. (2021) Glucose Metabolism and Use of Alternative Carbon Sources in Medically-Important Fungi. In Zaragoza, Ó., and Casadevall, A. (eds.), *Encyclopedia of Mycology*. Elsevier, Oxford, pp. 220-229.

Choi, H., Kim, S., Mukhopadhyay, P., Cho, S., Woo, J., Storz, G., and Ryu, S.E. 2001. Structural basis of the redox switch in the OxyR transcription factor. *Cell* **105**, 103-113.

Coelho, C. 2022. Itaconate or how I learned to stop avoiding the study of immunometabolism. *PLoS Pathog* **18**, e1010361.

Cordes, T., Michelucci, A., and Hiller, K. 2015. Itaconic Acid: The Surprising Role of an Industrial Compound as a Mammalian Antimicrobial Metabolite. *Annu Rev Nutr* **35**, 451-473.

Craven, S.H., Ezezika, O.C., Haddad, S., Hall, R.A., Momany, C., and Neidle, E.L. 2009. Inducer responses of BenM, a LysR-type transcriptional regulator from Acinetobacter baylyi ADP1. *Mol Microbiol* **72**, 881-894.

Cronan, J.E., Jr., and Laporte, D. 2005. Tricarboxylic Acid Cycle and Glyoxylate Bypass. *EcoSal Plus* **1**.

Dallakyan, S., and Olson, A.J. 2015. Small-molecule library screening by docking with PyRx. *Methods Mol Biol* **1263**, 243-250.

David, S., and Kroner, A. 2011. Repertoire of microglial and macrophage responses after spinal cord injury. *Nat Rev Neurosci* **12**, 388-399.

Degrandi, D., Hoffmann, R., Beuter-Gunia, C., and Pfeffer, K. 2009. The proinflammatory cytokine-induced IRG1 protein associates with mitochondria. *J Interferon Cytokine Res* **29**, 55-67.

Diaz, E., Ferrandez, A., and Garcia, J.L. 1998. Characterization of the hca cluster encoding the dioxygenolytic pathway for initial catabolism of 3-phenylpropionic acid in Escherichia coli K-12. *J Bacteriol* **180**, 2915-2923.

Emsley, P., Lohkamp, B., Scott, W.G., and Cowtan, K. 2010. Features and development of Coot. *Acta Crystallogr D Biol Crystallogr* **66**, 486-501.

Gautam, A., Dixit, S., Philipp, M.T., Singh, S.R., Morici, L.A., Kaushal, D., and Dennis, V.A. 2011. Interleukin-10 alters effector functions of multiple genes induced by Borrelia burgdorferi in macrophages to regulate Lyme disease inflammation. *Infect Immun* **79**, 4876-4892.

Hassett, D.J., and Cohen, M.S. 1989. Bacterial adaptation to oxidative stress: implications for pathogenesis and interaction with phagocytic cells. *Faseb j* **3**, 2574-2582.

Hersch, S.J., and Navarre, W.W. 2020. The Salmonella LysR Family Regulator RipR Activates the SPI-13-Encoded Itaconate Degradation Cluster. *Infect Immun* **88**.

Hess, B., Kutzner, C., van der Spoel, D., and Lindahl, E. 2008. GROMACS 4: Algorithms for Highly Efficient, Load-Balanced, and Scalable Molecular Simulation. *J Chem Theory Comput* **4**, 435-447.

Huang, J., Rauscher, S., Nawrocki, G., Ran, T., Feig, M., de Groot, B.L., Grubmuller, H., and MacKerell, A.D., Jr. 2017. CHARMM36m: an improved force field for folded and intrinsically disordered proteins. *Nat Methods* **14**, 71-73.

Jo, I., Chung, I.Y., Bae, H.W., Kim, J.S., Song, S., Cho, Y.H., and Ha, N.C. 2015. Structural details of the OxyR peroxide-sensing mechanism. *Proc Natl Acad Sci U S A* **112**, 6443-6448.

Jo, I., Kim, D., Bang, Y.J., Ahn, J., Choi, S.H., and Ha, N.C. 2017. The hydrogen peroxide hypersensitivity of OxyR2 in Vibrio vulnificus depends on conformational constraints. *J Biol Chem* **292**, 7223-7232.

Jo, I., Kim, D., No, T., Hong, S., Ahn, J., Ryu, S., and Ha, N.C. 2019. Structural basis for HOCl recognition and regulation mechanisms of HypT, a hypochlorite-specific transcriptional regulator. *Proc Natl Acad Sci U S A* **116**, 3740-3745.

Jo, S., Kim, T., Iyer, V.G., and Im, W. 2008. CHARMM-GUI: a web-based graphical user interface for CHARMM. *J Comput Chem* **29**, 1859-1865.

Jumper, J., Evans, R., Pritzel, A., Green, T., Figurnov, M., Ronneberger, O., Tunyasuvunakool, K., Bates, R., Zidek, A., Potapenko, A., Bridgland, A., Meyer, C., Kohl, S.A.A., Ballard, A.J., Cowie, A., Romera-Paredes, B., Nikolov, S., Jain, R., Adler, J., Back, T., Petersen, S., Reiman, D., Clancy, E., Zielinski, M., Steinegger, M., Pacholska, M., Berghammer, T., Bodenstein, S., Silver, D., Vinyals, O., Senior, A.W., Kavukcuoglu, K., Kohli, P., and Hassabis, D. 2021. Highly accurate protein structure prediction with AlphaFold. *Nature* **596**, 583-589.

Lahiri, A., Das, P., and Chakravortty, D. 2009. Salmonella Typhimurium: Insight into the multi-faceted role of the LysR-type transcriptional

regulators in Salmonella. *The International Journal of Biochemistry & Cell Biology* **41**, 2129-2133.

Lorenz, M.C., and Fink, G.R. 2001. The glyoxylate cycle is required for fungal virulence. *Nature* **412**, 83-86.

Maddocks, S.E., and Oyston, P.C.F. 2008. Structure and function of the LysR-type transcriptional regulator (LTTR) family proteins. *Microbiology (Reading)* **154**, 3609-3623.

Mahounga, D.M., Sun, H., and Jiang, Y.L. 2018. Crystal structure of the effector-binding domain of Synechococcus elongatus CmpR in complex with ribulose 1,5-bisphosphate. *Acta Crystallogr F Struct Biol Commun* **74**, 506-511.

Manso, I., Torres, B., Andreu, J.M., Menendez, M., Rivas, G., Alfonso, C., Diaz, E., Garcia, J.L., and Galan, B. 2009. 3-Hydroxyphenylpropionate and phenylpropionate are synergistic activators of the MhpR transcriptional regulator from Escherichia coli. *J Biol Chem* **284**, 21218-21228.

McFadden, B.A., and Purohit, S. 1977. Itaconate, an isocitrate lyase-directed inhibitor in Pseudomonas indigofera. *J Bacteriol* **131**, 136-144.

Menage, S., and Attree, I. 2014. Metabolism: pathogens love the poison. *Nat Chem Biol* **10**, 326-327.

Mirdita, M., Schütze, K., Moriwaki, Y., Heo, L., Ovchinnikov, S., and Steinegger, M. 2022. ColabFold - Making protein folding accessible to all. *bioRxiv*, 2021.2008.2015.456425.

Otwinowski, Z., and Minor, W. 1997. Processing of X-ray diffraction data collected in oscillation mode. *Methods Enzymol* **276**, 307-326.

Pronk, S., Pall, S., Schulz, R., Larsson, P., Bjelkmar, P., Apostolov, R., Shirts, M.R., Smith, J.C., Kasson, P.M., van der Spoel, D., Hess, B., and Lindahl, E. 2013. GROMACS 4.5: a high-throughput and highly parallel open source molecular simulation toolkit. *Bioinformatics* **29**, 845-854.

Ren, J., Sang, Y., Ni, J., Tao, J., Lu, J., Zhao, M., and Yao, Y.F. 2015. Acetylation Regulates Survival of Salmonella enterica Serovar Typhimurium under Acid Stress. *Appl Environ Microbiol* **81**, 5675-5682.

Sasikaran, J., Ziemski, M., Zadora, P.K., Fleig, A., and Berg, I.A. 2014. Bacterial itaconate degradation promotes pathogenicity. *Nat Chem Biol* **10**, 371-377.

Tangsudjai, S., Pudla, M., Limposuwan, K., Woods, D.E., Sirisinha, S., and Utaisincharoen, P. 2010. Involvement of the MyD88-independent pathway in controlling the intracellular fate of Burkholderia pseudomallei infection in the mouse macrophage cell line RAW 264.7. *Microbiol Immunol* **54**, 282-290.

Taylor, J.L., De Silva, R.S., Kovacikova, G., Lin, W., Taylor, R.K., Skorupski, K., and Kull, F.J. 2012. The crystal structure of AphB, a virulence gene activator from Vibrio cholerae, reveals residues that influence its response to oxygen and pH. *Mol Microbiol* **83**, 457-470.

Thomas, D.M., Francescutti-Verbeem, D.M., and Kuhn, D.M. 2006. Gene expression profile of activated microglia under conditions associated with dopamine neuronal damage. *FASEB J* **20**, 515-517.

Thompson, J.D., Gibson, T.J., Plewniak, F., Jeanmougin, F., and Higgins, D.G. 1997. The CLUSTAL_X Windows Interface: Flexible Strategies for Multiple Sequence Alignment Aided by Quality Analysis Tools. *Nucleic Acids Research* **25**, 4876-4882.

Uzzau, S., Brown, D.J., Wallis, T., Rubino, S., Leori, G., Bernard, S., Casadesus, J., Platt, D.J., and Olsen, J.E. 2000. Host adapted serotypes of Salmonella enterica. *Epidemiol Infect* **125**, 229-255.

Vagin, A., and Teplyakov, A. 2010. Molecular replacement with MOLREP. *Acta Crystallogr D Biol Crystallogr* **66**, 22-25.

van Kempen, M., Kim, S.S., Tumescheit, C., Mirdita, M., Söding, J., and Steinegger, M. 2022. Foldseek: fast and accurate protein structure search. *bioRxiv*, 2022.2002.2007.479398.

Varadi, M., Anyango, S., Deshpande, M., Nair, S., Natassia, C., Yordanova, G., Yuan, D., Stroe, O., Wood, G., Laydon, A., Zidek, A., Green, T., Tunyasuvunakool, K., Petersen, S., Jumper, J., Clancy, E., Green, R., Vora, A., Lutfi, M., Figurnov, M., Cowie, A., Hobbs, N., Kohli, P., Kleywegt, G., Birney, E., Hassabis, D., and Velankar, S. 2022. AlphaFold Protein Structure Database: massively expanding the structural coverage of protein-sequence space with high-accuracy models. *Nucleic Acids Res* **50**, D439-D444.

Winn, M.D., Ballard, C.C., Cowtan, K.D., Dodson, E.J., Emsley, P., Evans, P.R., Keegan, R.M., Krissinel, E.B., Leslie, A.G., McCoy, A., McNicholas, S.J., Murshudov, G.N., Pannu, N.S., Potterton, E.A., Powell, H.R., Read, R.J., Vagin, A., and Wilson, K.S. 2011.

Overview of the CCP4 suite and current developments. *Acta Crystallogr D Biol Crystallogr* **67**, 235-242.

VI. 국문초록

LPS 에 의해 활성화된 대식세포는 침입하는 병원균에 대응하기 위해 파고솜에서 이타콘산을 생성한다. 이타콘산은 병원균의 글리옥실산 회로의 첫 번째 효소인 isocitrate lyase 를 경쟁적으로 저해한다. 이타콘산 스트레스를 방어하기 위해 박테리아는 세균의 LysR 형 전사 조절인자인 RipR 을 이용한다. 그러나 어떤 분자가 세균의 병인 발생에서 RipR 을 활성화하는지는 여전히 알려져 있지 않다. 본 연구에서는 세포 내 병원체 살모넬라에서 RipR 의 조절 도메인(RD)의 결정 구조를 확인하였다. RipR RD 구조는 두 서브 도메인 사이에 리간드 결합 부위를 갖는 전형적인 이량체 배열을 보였다. ITC 실험을 통해 이타콘산 스트레스에 반응하여 세포 내 수치가 증가하는 아이소시트르산 분자가 RipR 의 생리학적 리간드로 확인되었다. 우리는 또한 3-페닐프로피온산이 이타콘산 스트레스에 대한 박테리아의 저항을 유의미하게 감소시킨다는 것을 발견했다. 일관되게, 3-페닐프로피온산 복합 구조는 화합물이 RipR 리간드 결합 부위에 길항적으로 결합되어 있음을 보여주었다. 본 연구는

세균이 인체 면역 시스템 내의 이타콘산 스트레스에서 살아남는 분자적 기전을 제시하였다. 살모넬라균이 세균의 대사경로를 방해하는 이타콘산을 방어함으로써 대식세포의 파고솜에서 살아남는 방법을 설명하는 생화학적 활성을 밝히기 위한 추가 연구가 필요하다.

주요어 : 이타콘산, LysR 형 전사조절인자, 아이소시트르산, 글라이옥실산 회로, 3-페닐프로피온산, 결정 구조

학번 : 2020-25807